TANGENCY BIFURCATIONS OF GLOBAL POINCARÉ MAPS

CLARE M. JUDD*, PIETER. J. COLLINS†, BERND KRAUSKOPF*, AND HINKE M. OSINGA*

August 2007

Abstract. One tool to analyze the qualitative behavior of a periodic orbit of a vector field in $\mathbb{R}^n$ is to consider the Poincaré return map to an $(n-1)$-dimensional section. The image under the Poincaré map of points on this section that lie near the periodic orbit is obtained by following the orbits under the flow of the vector field until the next (local) intersection. It is well known that the Poincaré map defined on a section transverse to a periodic orbit is a diffeomorphism locally near the periodic orbit. However, in practice, often an arbitrary global Poincaré section is taken. Generically, there are points where the flow is tangent to the Poincaré section, and these give rise to discontinuities of the Poincaré map. In fact, the orbits of some points may not even return to the section, in which case the Poincaré map is not defined at all.

In this paper we study tangency bifurcations of invariant manifolds of Poincaré maps on global sections of vector fields in $\mathbb{R}^2$ and $\mathbb{R}^3$. At such a bifurcation the manifold becomes tangent to the section, which results in a qualitative change of the Poincaré map while the underlying flow itself does not undergo a bifurcation. Using tools from singularity theory, we present all normal forms of the codimension-one tangency bifurcations in the neighborhood of the respective tangency point. The study of these bifurcations is motivated by and illustrated with the examples of the (unforced) Van der Pol oscillator and a system modeling a semiconductor laser with optical injection. Finally, we present a framework for the generalization of our normal form results to arbitrary dimension and codimension.

Key words. Poincaré map, quadratic and cubic tangency, flowbox, normal forms, singularity theory.

AMS subject classifications. 37C10, 37G25, 58K50.

1. Introduction.

In 1892 Henri Poincaré introduced the idea of a return map of a vector field — today generally referred to as a *Poincaré map* — while he was studying a restriction of the three-body problem [30]. His aim was to find the motion of three bodies (one having negligible mass compared with the other two, for example, the Sun, Earth and Moon), given only their initial positions, velocities, and masses. His work was fundamental for both the local and global analysis of nonlinear dynamical systems. In particular, he studied periodic orbits and their stability and introduced the first return map to a given local section as a new tool. In this setting the section in phase space is chosen transverse to the periodic orbit, and one considers the map that is defined locally on the section by following the flow until it returns back to the section. The periodic orbit of the system corresponds to a fixed point of this Poincaré map. Since the Poincaré map is a diffeomorphism (a smooth map with a smooth inverse) in a neighborhood of this fixed point, the existence and stability analysis of periodic orbits in the full phase space reduces to the study of fixed points of local

*Centre for Applied Nonlinear Mathematics, Department of Engineering Mathematics, University of Bristol, Queen's Building, Bristol BS8 1TR, UK (Clare.Judd@bristol.ac.uk). H.M.O. was supported by an Advanced Research Fellowship grant from the Engineering and Physical Sciences Research Council (EPSRC).

†Centrum voor Wiskunde en Informatica, Kruislaan 413, 1098 SJ Amsterdam, The Netherlands. This author was supported by a Vidi grant of the Nederlandse Organisatie voor Wetenschappelijk Onderzoek (NWO).

diffeomorphisms. This fact is used in the bifurcation analysis of periodic orbits in standard textbooks such as [15, 24, 33].

Today, the Poincaré map is a much-used tool in theoretical studies and in the evaluation of experiments alike. Generally speaking, one studies attractors and other invariant sets that one obtains by considering only the intersection points of the flow with a prespecified Poincaré section. One way of obtaining such a representation is to plot measured quantities (for example, position, velocity, voltage or current) whenever a designated quantity has a particular value, for example, when it crosses its average. Another common choice is to consider a section in the space of the first derivative of the flow and to plot the position of successive maxima/minima of the system; such maps can be seen, for example, in [1, 31]. In this way, one can illustrate classic transitions, such as the period-doubling route to chaos or the break-up of an invariant torus.

The above discussion already shows that in practice one typically chooses a *global Poincaré section* on a codimension-one submanifold of the flow. A common choice is a (hyper)plane defined by one of the variables having a fixed value. The question arises what the properties are of the *global Poincaré map*, which is defined as the first return to the global section.

A special case is that of a stroboscopic map of a periodically forced system with angular frequency ω; well-known examples (see, for example, [15, 33]) include the forced damped pendulum, the forced Van der Pol and the forced Duffing oscillators. A periodically forced system can be written as an autonomous vector field by considering time t as another variable, which is, hence, periodic with period $2\pi/\omega$. The Poincaré section is then taken at $t = 2\pi/\omega$, so that the Poincaré map records the variables at regular time intervals. In a mechanical experiment, this can be achieved by stroboscopic illumination with the forcing frequency, hence, the name stroboscopic map; see, for example, [5, 19]. Since the section is effectively taken in time and not in space, each orbit intersects the global section defined by $t = 2\pi/\omega$ and does so transversely. This means that the stroboscopic map is a well-defined global diffeomorphism on the entire section.

By contrast, for a vector field that is not periodically forced one cannot find a global section on which the Poincaré map is a global diffeomorphism. Given a general autonomous vector field and any Poincaré section Σ, there exists a non-empty set of codimension one — which we call the *tangency locus* — where the vector field is tangent to Σ, that is, the flow is not transverse to the section. Furthermore, there may be orbits that may not return to the section in forward or backward time. These two obstructions were already known to Birkhoff [3] who considered the problem of finding a Poincaré map in the context of Hamiltonian systems. His goal was to find a so-called complete section that is intersected by all trajectories, so that the Poincaré map gives information about the entire dynamics. Birkhoff's result is that the Poincaré map is well defined, smooth and complete if the section is such that the tangency locus is invariant under the first return; one also speaks of a Birkhoff section [9]. In this case it is sufficient to consider the Poincaré map on a compact region that is bounded by the tangency locus. For a two-degree-of-freedom Hamiltonian system one obtains an area preserving map of the plane, by means of restricting to a fixed-energy surface. However, for arbitrary Hamiltonian systems the condition that the tangency locus is invariant under the first return is not necessarily satisfied. To deal with this more general Hamiltonian situation, Dullin and Wittek [9] generalized Birkhoff's result by constructing what they call a W-section, which guarantees a weaker form

of completeness in the sense that orbits either return to the W-section in finite time or have a limit in the W-section as time goes to infinity. Analyzing the properties of the associated Poincaré map requires the study of geometric properties of the flow in phase space in relation to the energy surface [4].

We consider here the properties of the Poincaré map on a global section of a generic autonomous vector field, without any special properties such as a Hamiltonian structure or preserved symmetries. Typically, there are regions of the section where the Poincaré first return map can be defined locally as a diffeomorphism by considering the k-th return map to the global section for a suitable fixed k. Such regions are bounded by the tangency locus. Namely, the k-th return map is discontinuous across the tangency locus. This fact was used in [20] to explain the emergence of an increasing number of discontinuities of the one-dimensional map approximation associated with a chaotic attractor, such as that of the Rössler system. However, when one allows the number of intersections k with the section to vary across the tangency locus, then the Poincaré map can be extended as a continuous map to an adjacent region. How the number k must be changed to ensure continuity of the Poincaré map can be determined from the condition that the integration time be continuous; see also [9]. This idea was used in [8] to compute one-dimensional invariant manifolds of the global Poincaré map across the tangency locus. By continuing orbit segments (with the associated integration time) as two-point boundary value problems it is possible to compute one-dimensional invariant manifolds of the global Poincaré map across the tangency locus without the need for manually changing the number k of returns to the section; see [11] for details and examples.

The specific topic addressed in this paper is the characterization of bifurcations of a global Poincaré map that do not correspond to bifurcations of the underlying flow. Such topological changes of the Poincaré map can be brought about either by changing a system parameter so that an invariant object changes in such a way that its intersection with the section is affected, or equivalently by changing the position of the section in the flow. Indeed, one needs to take some care to avoid drawing wrong conclusions from topological changes of phase portraits in a Poincaré section. A concrete example is the appearance of extra branches of intersections with a fixed Poincaré section of a one-parameter family of periodic orbits. This may simply be due to the periodic orbit changing shape in the full phase space, which does not correspond to a bifurcation of the flow. The emergence of extra branches in a Poincaré section typically happens, for example, when the orbit approaches a saddle-focus equilibrium [14]. Another example is the intersection of an invariant torus with a section, which can take different forms, as is discussed in detail in section 4.

The situation may be even more complicated in some applications. An example is the study by Peikert and Sadlo [28, 29] of one-dimensional invariant manifolds in a two-dimensional section through a vortex ring associated with a river power plant. The authors refer to "seemingly ring-shaped lobes [as] an artefact of the slice plane which does not follow well the curved center line of the structure" [29, Sec 5.2]. Indeed, such "lobes" arise due to the way the section intersects a corresponding two-dimensional manifold, and this depends on the exact position of the section. In particular, the study of changes of the invariant set with the position of the section is important for the interpretation of experimental measurements, such as the two-dimensional sections through a vortex structure by means of a laser sheet [12].

We consider the generic bifurcations of a smooth invariant manifold of dimension ℓ as it interacts with a Poincaré section of a generic vector field with an n-dimensional

phase space. We call these bifurcations *tangency bifurcations*, because they are generated by orbits that are tangent to the section at the bifurcation point. We analyze the tangency bifurcations locally in a generic framework, which means that there are no equilibria in the section. Therefore, we may consider a flowbox in a suitable neighborhood of the bifurcation point, which is simply a domain in phase space that is bounded by orbit segments and transverse codimension-one in- and out-sets. We use the Flowbox Theorem [27] and to 'straighten out' the flow by mapping it to the standard flowbox with parallel flow. Subsequently, we apply coordinate changes to map the section to a standard form as motivated by singularity theory; the key here is to show that the coordinate changes can be chosen to preserve the flow lines in the standard flowbox. As a result, we obtain normal forms for the unfoldings of tangency bifurcations in terms of parametrized families of curved Poincaré sections in the standard flowbox. Specifically, we treat all generic tangency bifurcations of codimension-one for $n \leq 3$, that is, for Poincaré sections of dimension one and two. To this end, we first consider tangency bifurcations of invariant manifolds in a one-dimensional Poincaré section of a two-dimensional flow, before concentrating on the important case of tangency bifurcations in a two-dimensional Poincaré section of a vector field in $\mathbb{R}^3$. We also discuss briefly how the notion of a tangency bifurcation can be be generalized for arbitrary n and ℓ.

Our normal form investigations are motivated by and illustrated with examples of how the different tangency bifurcations manifest themselves in Poincaré maps of concrete vector fields arising in applications. Namely, we consider here the two-dimensional unforced Van der Pol oscillator, and a three-dimensional vector field model of a semiconductor laser with optical injection [36].

The approach of using methods from singularity theory to classify the dynamics of a special class of systems has been employed for different but somewhat related systems, notably impacting systems [7] and noninvertible maps (endomorphisms) of the plane [10, 16, 23]. However, closest in spirit is the work of Sotomayor and Teixeira who study generic flows on a manifold with a codimension-one boundary, namely two-dimensional flows in [34] and three-dimensional flows in [32]. Sotomayor and Teixeria work in a completely general setting and investigate what conditions on the vector field and the section are needed for structural stability of the interaction between the flow and the boundary. Because in our setup the Poincaré section plays the role of their boundary, we can use their genericity results in our context. There are a number of differences between their work and what is presented here. Firstly, Sotomayor and Teixeira do not consider the flow on the 'outside' of the boundary, while we are interested in the flow on both sides of the Poincaré section. Secondly, we consider bifurcations of a 'local piece' of an invariant one- or two-dimensional manifold in a local flowbox around a bifurcation point. This piece of manifold could be part of a periodic orbit, invariant torus or a stable or unstable manifold of a saddle object. While the tangency bifurcation remains locally the same, its global manifestation depends on the type of invariant manifold one is considering. For example, Sotomayor and Teixeira consider as separate the two cases that a periodic orbit or a one-dimensional separatrix has a tangency with the boundary, which we interpret as manifestations of the same interaction with the Poincaré section. Moreover, two-dimensional invariant manifolds were not considered in [32].

This paper is organised as follows. In section 2 we discuss the motivation behind this paper and outline the problems that arise from globalising a local Poincaré map; here we also provide formal definitions. In section 3 we consider the tangency bi-

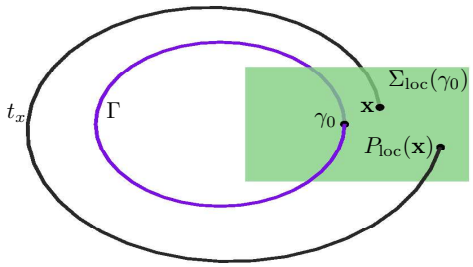

FIG. 1. *A periodic orbit* Γ *intersecting a local section* $\Sigma_{\rm loc}(\gamma_0)$ *at the point* γ_0. *The local Poincaré map* $P_{\rm loc}$ *takes* $\mathbf{x}$ *to the next local intersection* $P_{\rm loc}(\mathbf{x})$ *with* $\Sigma_{\rm loc}(\gamma_0)$.

furcation with a global Poincaré section of a two-dimensional flow, which is due to a quadratic tangency of an invariant manifold; this case is illustrated with the Van der Pol oscillator. Section 4 then deals with quadratic tangencies of invariant manifolds with a two-dimensional Poincaré section of a three-dimensional flow; a model of a semiconductor laser with optical injection serves as a concrete example. In section 5 we consider the case of cubic tangency bifurcations, which involve an orbit on an invariant manifold that has a cubic tangency with the Poincaré section of a three-dimensional flow; what this bifurcation looks like in practice is again illustrated with the example of a semiconductor laser with optical injection. Section 6 discusses the general case of a tangency bifurcation of an ℓ-dimensional manifold with a global Poincaré section of an n-dimensional flow. Finally, in section 7 we draw some conclusions and discuss directions for future research.

2. Background and Motivation. Many readers will be familiar with the concept of a Poincaré map defined on a local section transverse to a periodic orbit. Consider a vector field

$$\dot{\mathbf{x}} = f(\mathbf{x}, \lambda), \quad \mathbf{x} \in X, \quad \lambda \in \mathbb{R}^m, \tag{2.1}$$

where X is the phase space, λ is a (vector-valued) parameter, and $f : X \to X$ is sufficiently smooth. For the purposes of this paper $X = \mathbb{R}^n$ where we mostly consider the cases $n = 2$ or $n = 3$. The flow associated with (2.1) is denoted by Φ, so that the orbit or trajectory through x is defined as

$$\mathcal{O}(x) = \{\Phi^t(x) \mid t \in \mathbb{R}\}. \tag{2.2}$$

We assume now that (2.1) has a periodic orbit Γ for some value of λ. Note that generically Γ is part of a (λ-dependent) family, but for the moment we consider the parameter λ as fixed. To obtain the standard definition of a local Poincaré map $P_{\rm loc}$ one chooses an $(n-1)$-dimensional submanifold Σ that intersects Γ transversely at an intersection point γ_0. The Poincaré map is then defined in some neighborhood $\Sigma_{\rm loc}(\gamma_0)$ of γ_0; see, for example, [24, 27]. A point $\mathbf{x} \in \Sigma_{\rm loc}(\gamma_0)$ is taken by the flow Φ to the next intersection of the forward trajectory $\{\Phi^t(\mathbf{x}) \mid \forall t \geq 0\}$ with $\Sigma_{\rm loc}(\gamma_0)$; see also figure 1. That is,

$$\begin{aligned} P_{\rm loc} : \Sigma_{\rm loc}(\gamma_0) &\to \Sigma_{\rm loc}(\gamma_0) \\ \mathbf{x} &\mapsto P_{\rm loc}(\mathbf{x}) := \Phi^{t_x}(\mathbf{x}), \end{aligned} \tag{2.3}$$

where $t_{\mathbf{x}} = \min\{t > 0 \mid \Phi^t(\mathbf{x}) \in \Sigma_{\text{loc}}(\gamma_0)\}$ is the time to the next local intersection. Note that γ_0 is a fixed point of P_{loc} and that $t_{\mathbf{x}}$ is close to the period of the periodic orbit Γ. Since the section Σ is chosen transverse to Γ at γ_0, it is always possible to choose $\Sigma_{\text{loc}}(\gamma_0)$ such that P_{loc} is a well-defined diffeomorphism on $\Sigma_{\text{loc}}(\gamma_0)$.

Locally near γ_0 the dynamics of the vector field f are equivalent to the dynamics of P_{loc} on $\Sigma_{\text{loc}}(\gamma_0)$, so that the local Poincaré map allows the study of basic bifurcations of the periodic orbit Γ; see, for example, [15, 24, 33]. However, in many applications one is interested not only in a periodic orbit Γ but in more general invariant sets, including invariant tori and chaotic attractors. Therefore, one often considers some suitably chosen 'large' and generally unbounded *global section* in phase space. For the purpose of this paper, we call Σ a global Poincaré section if it is the image of a smooth embedding

$$F : \mathbb{R}^{n-1} \to \mathbb{R}^n, \tag{2.4}$$

where we assume that $F(\mathbb{R}^{n-1})$ divides the phase space $\mathbb{R}^n$ into two disjoint parts. In other words, a global Poincaré section $\Sigma = F(\mathbb{R}^{n-1})$ is a smooth manifold of dimension $(n-1)$ that is unbounded in all directions. Specifically, Σ is the unbounded image of the real line for $n = 2$ and of a two-dimensional plane for $n = 3$. It is common in applications to choose Σ simply as an $(n-1)$-dimensional hyperplane.

The *global Poincaré map* on the global section Σ is then defined as in (2.3), except that we now consider P on the entire global section Σ, that is,

$$\begin{aligned} P : \Sigma &\to \Sigma \\ \mathbf{x} &\mapsto P(\mathbf{x}) := \Phi^{t_{\mathbf{x}}}(\mathbf{x}), \end{aligned} \tag{2.5}$$

where $t_{\mathbf{x}}$ is the time to first intersection with Σ; note that P is well defined at $\mathbf{x}$ if $0 < \inf\{t > 0 \mid \Phi^t(\mathbf{x}) \in \Sigma\} < \infty$.

As can already be inferred from figure 1, a global section Σ typically has $k \geq 2$ intersections with a periodic orbit Γ. (Note that generically there is an even number of points in $\Gamma \cap \Sigma$.) In other words, the local Poincaré map P_{loc} defined on $\Sigma_{\text{loc}}(\gamma_0)$ coincides with the restriction to $\Sigma_{\text{loc}}(\gamma_0)$ of the kth iterate of the global Poincaré map as defined by (2.5). Indeed, P^k is a local diffeomorphism near any of the (transverse) intersection points of Γ with Σ.

It turns out that the global Poincaré map as defined by (2.5) is a diffeomorphism on the whole of Σ that describes the entire dynamics on $\mathbb{R}^n$ only under rather severe conditions (see, for example, [3, 26]), namely, only when

1. the flow Φ of (2.1) is transverse to Σ at every point $\mathbf{x} \in \Sigma$;
2. the forward orbit and the backward orbit through every point $\mathbf{x} \in \Sigma$ both have another intersection with Σ; and
3. every orbit of (2.1) intersects Σ.

Indeed, these conditions are typically not satisfied because of the following result.

THEOREM 2.1. *For a generic vector field on a given phase space it is not possible to find a global Poincaré section Σ to which all points return and that is everywhere transverse to the flow, unless the phase space can be written as $\mathbb{S}^1 \times \Sigma$.*

Theorem 2.1 is proved in [37] in two basic steps; see also [3, 6, 9, 26]. The first step is to show that if a global Poincaré section with the above properties exists then the phase space X is topologically equivalent to the suspension manifold $\Sigma \times [0,1]/\sim$. Here, the quotient is taken with respect to the equivalence relation $\sim$, where $(x_1, 0) \sim (x_2, 1)$ for $x_1, x_2 \in \Sigma$, $x_1 \neq x_2$, if $x_2 = P(x_1)$. The second step of the proof is to show that

if Σ is a smooth manifold on which P is a diffeomorphism then $[0,1] \times \Sigma/\sim$ can be written as $\mathbb{S}^1 \times \Sigma$.

An immediate consequence of Theorem 2.1 is the following.

COROLLARY 2.2. *A global Poincaré map P that is a diffeomorphism on a global section Σ can be found for a generic vector field on a given phase space if, and only if, the vector field is equivalent to a periodically forced system.*

Periodically forced vector fields are an important subclass with well-known examples such as the forced damped pendulum, the forced Van der Pol equations and the forced Duffing oscillator [15, 33]. The global Poincaré map in the sense discussed here is given as the stroboscopic map, that is, as the time-$2\pi/\omega$ map. The fact that the stroboscopic map is a global diffeomorphism is a particularly nice property of periodically forced vector fields. However, according to Corollary 2.2 this property is very special. In particular, for a general (that is, not a periodically forced) vector field there are points where the vector field is tangent to the global section Σ. This can already be deduced from the case of a section through a periodic orbit Γ. If one considers two consecutive (transverse) intersection points γ_0 and γ_1 of Γ with Σ, then the flow points in opposite directions (with respect to Σ) near γ_0 and γ_1, respectively. By continuity of the flow, we must have at least one point on Σ where the vector field is tangent to the section. We define the *tangency locus* C as

$$C := \{\mathbf{x} \in \Sigma \mid f(\mathbf{x}) \cdot \vec{n}_\Sigma(\mathbf{x}) = 0\}\,, \tag{2.6}$$

where $\vec{n}_\Sigma(\mathbf{x})$ is the unit normal to Σ at the point $\mathbf{x}$. Note that if Σ is a hyperplane the normal $\vec{n}_\Sigma(\mathbf{x})$ does not depend on $\mathbf{x}$. For the remainder of this paper we assume that $C \neq \emptyset$. It follows from the Implicit Function Theorem [35] that C consists of smooth codimension-one submanifolds of Σ. That is, for a one-dimensional section Σ ($n = 2$) the tangency locus C is generically a set of isolated points. For a two-dimensional section Σ ($n = 3$) it consists of smooth curves. Furthermore, in a two-dimensional section Σ there may be points of C where the flow has a cubic tangency (that is, a cusp singularity) with Σ; such points are generically isolated. These genericity statements follow from results by Sotomayor and Teixeira in [34, 32] on flows on two- and three-dimensional manifolds with boundary.

The importance of the tangency locus C lies in the realization that any kth-return map to Σ for any $k \geq 0$, that is, the Poincaré map P as defined by (2.5) or its kth iterate, is discontinuous across C; this was already noted by Birkhoff [3] in the context of Hamiltonian systems. The reason for this discontinuity is that the number of intersection with the section Σ changes due to the quadratic tangency; see also section 3.1. We remark that a kth-return map can be extended continuously across C; namely, by changing the number of global intersections and considering the $(k \pm 1)$th-return map in the adjoining region. The required number of global intersections is determined by the condition that the time $t_{\mathbf{x}}$ to the next (local) intersection depends continuously on the point $\mathbf{x}$ across C [8]; see also [9]. This approach of extending a Poincaré map across C by continuation of the entire orbit segment from Σ back to Σ, which includes the integration time $t_{\mathbf{x}}$, is especially useful when one wants to compute invariant manifolds of global Poincaré maps [11]. Note that a thus extended Poincaré map is only continuous across C, but not smooth. In other words, the existence of a tangency locus is indeed an obstacle to finding a Poincaré map that is a global diffeomorphism.

We consider here tangency bifurcations of the Poincaré map P on a global section Σ, which are characterized by the interaction of an invariant manifold M with the

tangency locus $C \subset \Sigma$. The first step is to define an appropriate notion of topological equivalence.

DEFINITION 2.3. *Given two flows on two open neighborhoods U_1 and U_2 of $\mathbb{R}^n$ and $(n-1)$-dimensional smooth sections $\Sigma_1 \subset U_1$ and $\Sigma_2 \subset U_2$ with tangency loci C_1 and C_2, respectively. Suppose further, that there are ℓ-dimensional invariant manifolds $M_1 \in U_1$ and $M_2 \in U_2$. We say that the flow on U_1 is* Σ-M-topologically equivalent *to that on U_2 if there exists a homeomorphism $h : U_1 \to U_2$ such that*

(E1) h maps orbits in U_1 to orbits in U_2 and respects the direction of time;

(E2) h maps Σ_1 to Σ_2 and C_1 to C_2; and

(E3) $h|_\Sigma$ maps $M_1 \cap \Sigma_1$ to $M_2 \cap \Sigma_2$.

Note that (E1) ensures that h maps M_1 to M_2. For notational convenience, we refer to Σ-M-topological equivalence simply as topological equivalence in what follows. Similarly, we refer to the orbits of a flow on an open set U relative to $\Sigma, M \subset U$ simply as a phase portrait.

Following standard ideas of bifurcation theory [15, 24], we say that a phase portrait is structurally stable if any sufficiently close phase portrait is topologically equivalent. Here closeness between phase portraits is given by the C^1-topology of the underlying vector fields and C^1-distance between the respective sections and invariant manifolds; compare with [32, 34]. Consequently, a bifurcation takes place when a phase portrait is not structurally stable. In the usual way, two unfoldings of a bifurcation are said to be topologically equivalent if respective phase portraits are topologically equivalent and the underlying family of homeomorphism can be chosen to depend continuously on the parameters.

Clearly bifurcations of the underlying flow in the usual sense (meaning that (E1) is violated) are also bifurcations of the Poincaré map P in the sense of Definition 2.3; these bifurcations are covered by standard bifurcation theory. However, there are new types of bifurcations in the sense of Definition 2.3, namely those that correspond to violation of (E2) and/or (E3). The interest here is on a class of such bifurcations — the tangency bifurcations — that are due to a qualitative change of $M \cap \Sigma$. Tangency bifurcations do not involve equilibria in Σ, so that we can consider the phase portrait in a flowbox near the interaction of the invariant manifold with the section. A flowbox does not contain any equilibria and is characterized by an in-set I and an out-set O transverse to the flow, with 'sides' that consist of orbit segments. According to the Flowbox Theorem [27], the vector field in any given flowbox is conjugate (by means of a coordinate transformation that is as smooth as the vector field f) to parallel flow in the standard flowbox, which we define here for definiteness as

$$\begin{cases} \dot{u} &= 1, \\ \dot{v} &= 0, \end{cases} \tag{2.7}$$

where $u \in [-1, 1]$ and $v \in [-1, 1]^{n-1}$. It follows that the standard in-set and the standard out-set are

$$I = \{u = -1\} \quad \text{and} \quad O = \{u = +1\}. \tag{2.8}$$

The basic idea behind transforming a given flowbox, such as the example shown in figure 4, to the standard flowbox is that the flow lines are 'straightened out'. In the present setting, this means that the section Σ becomes curved. In other words, a normal form as considered here consists of a suitable family of curved sections that interact with a fixed invariant manifold, which is determined by a prespecified subset of the in-set I.

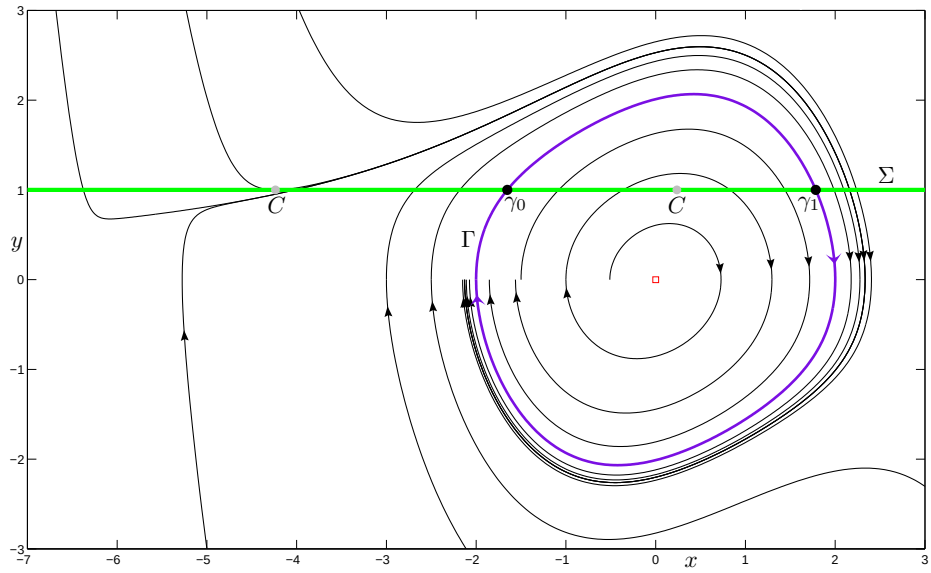

FIG. 2. *Phase portrait of the (unforced) Van der Pol oscillator (3.1) for $\mu = 0.25$ with a global Poincaré section Σ_1 (green line) at $y = 1$. The periodic orbit Γ (purple) intersects Σ_1 at the two points γ_0 and γ_1. The flow is tangent to Σ at the points denote by C.*

3. Two-dimensional flows. Let us now focus on the Poincaré map on a one-dimensional global section of a two-dimensional vector field. We begin by explaining the main concepts with a concrete example in section 3.1, before presenting a general normal-form result in section 3.2.

3.1. The (unforced) Van der Pol oscillator. As a concrete motivating example we consider the (unforced) Van der Pol oscillator [18, 33] of an RLC circuit, which is defined as the two-dimensional vector field

$$\begin{cases} \dot{x} &= y, \\ \dot{y} &= \mu(1-x^2)y - x, \end{cases} \tag{3.1}$$

where $\mu = 0.25$ is used throughout this paper. For this value of μ system (3.1) has an attracting periodic orbit Γ. We choose the global Poincaré section as the horizontal line

$$\Sigma = \Sigma_s := \{(x, y) \in \mathbb{R}^2 \mid y = s\}, \tag{3.2}$$

for some constant $s \in \mathbb{R}$. Figure 2 shows how the global section Σ (green) for $s = 1$ intersects the periodic orbit Γ transversely in two points, γ_0 and γ_1. Recall that a transverse intersection of Σ with Γ always leads to at least two intersection points, regardless of the choice of Σ. Near γ_0 the flow is upward through Σ, while near γ_1 it points down; at the points C the flow is tangent to Σ. Using equations (3.1) and (3.2), the points C at which the flow is tangent to Σ satisfy

$$\dot{y}\big|_{y=s} = 0 \quad \Leftrightarrow \quad \mu(1-x^2)y - x\big|_{y=s} = 0,$$

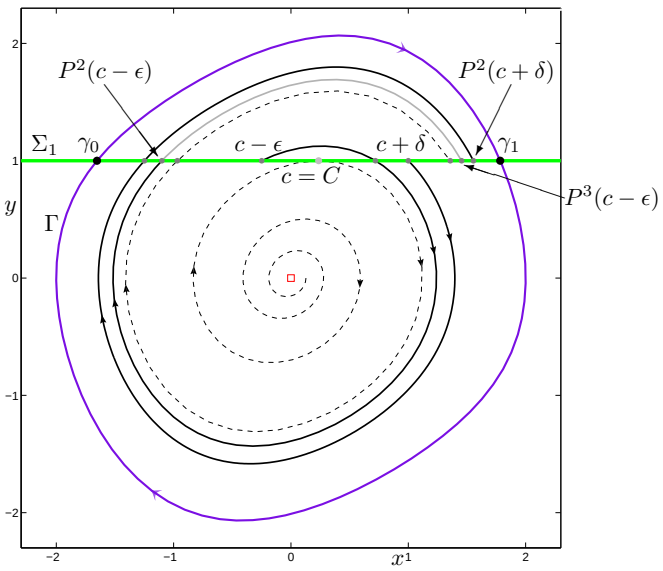

FIG. 3. *Illustration of the discontinuity of P^2 for the Van der Pol oscillator (3.1) across a tangency point $c \in \Sigma_1$; compare with figure 2.*

so that

$$C = C(s) = \begin{cases} \{(0,0)\}, & \text{if } s = 0, \\ \left\{ \left(\frac{1 \pm \sqrt{1+4\mu^2 s^2}}{-2\mu s}, s \right) \right\}, & \text{if } s \neq 0. \end{cases}$$

As is clear from this formula, changing the section a little (that is, a sufficiently small change of $s \neq 0$) does not lead to a qualitative change of the tangency set C. The two tangency points $(-2 \pm \sqrt{5}, 1)$ for $s = 1$ are labeled C in figure 2. From the figure we can observe that the first intersection with Σ of the forward orbit $\mathcal{O}^+(\mathbf{x})$ of a point $\mathbf{x}$ below Σ (except for the equilibrium at the origin) always lies to the left of the tangency point $(-2 + \sqrt{5}, 1)$. In fact, in this case $\mathcal{O}^+(\mathbf{x})$ also always lies to the right of the other tangency point $(-2 - \sqrt{5}, 1)$. By contrast, the forward orbit of a point $\mathbf{x}$ above Σ either intersects to the left of $(-2 - \sqrt{5}, 1)$ or to the right of $(-2 + \sqrt{5}, 1)$, which depends on whether the orbit starts to the right or to the left of the backward orbit of the tangency point $(-2 - \sqrt{5}, 1)$. Note that this backward orbit divides the space into orbits that intersect Σ and orbits that miss.

Near γ_0 we can define a local Poincaré map P_{loc} on a local section $\Sigma_{\text{loc}}(\gamma_0) \subset \Sigma$ and similarly we can define P_{loc} near γ_1 on $\Sigma_{\text{loc}}(\gamma_1) \subset \Sigma$. Since there are two transverse intersection of Γ with Σ, we have $P_{\text{loc}} = P^2$ on both $\Sigma_{\text{loc}}(\gamma_0)$ and $\Sigma_{\text{loc}}(\gamma_1)$, where P is the global Poincaré map as defined by (2.5). Figure 3 illustrates that P^2 is indeed not a continuous map on the whole of Σ, but is discontinuous at C. To see this we consider the tangency point $c := (-2 + \sqrt{5}, 1) \in C$. The image $P^2(c + \delta)$ of any point $c + \delta \in \Sigma_s$, for $\delta \geq 0$, lies closer to γ_1 than $c + \delta$. (The only exception is $P^2(\gamma_1) = \gamma_1$.) Note that $P^2(c)$ is the limit of $P^2(c + \delta)$ as $\delta \to 0$ and it lies closer to γ_1 than c. Now consider a point $c - \epsilon \in \Sigma$ for $\epsilon > 0$ small. As is shown in figure 3, the image $P^2(c - \epsilon)$ lies closer to γ_0 than $c - \epsilon$. In the limit of $\epsilon \to 0$ the image $P^2(c - \epsilon)$

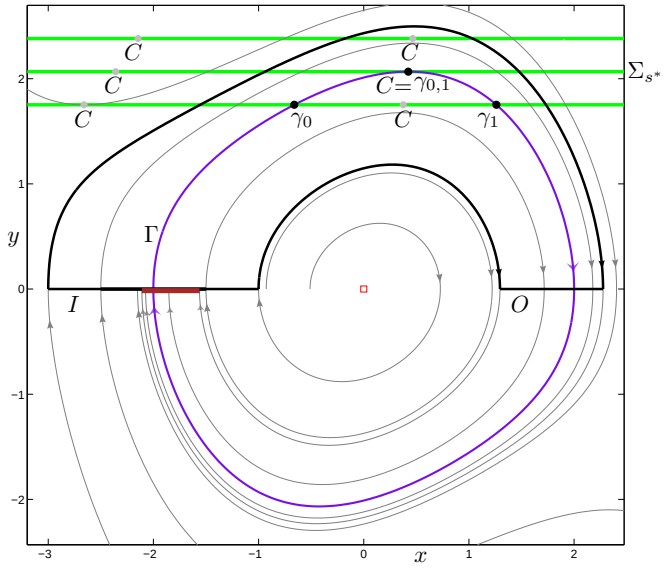

FIG. 4. *A flowbox for the Van der Pol oscillator (3.1) near the quadratic tangency of the periodic orbit* Γ *with the section* Σ_{s^*}*; the three topologically different choices for* Σ_s *(green lines) are* $s = 1.7518$*,* $s = 2.0670$*, and* $s = 2.3822$*; compare with figure 2.*

converges to $P^1(c)$ rather than to $P^2(c)$. Hence, P^2 is discontinuous across c.

It is straightforward to see that the discontinuity of P^2 is due to a discontinuity of the global Poincaré map P itself. Namely, we have that

$$\lim_{\epsilon \to 0} P(c - \epsilon) = c \neq P(c) = \lim_{\delta \to 0} P(c + \delta).$$

Note that this involves a discontinuity of the integration time, namely, the first-return time $t_{(c-\epsilon)}$ associated with $P(c - \epsilon)$ goes to 0 for $\epsilon \to 0$, while there is a finite integration time associated with the orbit segment connecting c with $P(c)$. As can be seen from figure 3, the continuous extension of $P_{\rm loc} = P^2$ from $\Sigma_{\rm loc}(\gamma_1)$ across the point c to $\Sigma_{\rm loc}(\gamma_0)$ is the map P^3. In particular, for this extension the integration time back to a local neighborhood of the section is continuous; see also [8, 11].

We now consider the interaction of the family of sections Σ_s with the periodic orbit Γ, that is, with an invariant manifold of the flow. As is shown in figure 4, a codimension-one bifurcation of the Poincaré map occurs for the specific value s^* of s where Γ has a quadratic tangency with the section Σ_{s^*}; numerically we find that $s^* \approx 2.0670$. For $s < s^*$ there are two transverse intersection points of Γ with Σ_s, as is the case in figures 2 and 3. For $s > s^*$, on the other hand, Γ has no intersections at all with Σ_s, so that the Poincaré map P does not give any information on the dynamics of Γ in this case.

To analyze the situation we consider a flowbox that includes part of the periodic orbit Γ near the tangency point with Σ; see figure 4 where the flowbox is indicated by thick black lines. Note that the periodic orbit Γ inside the flowbox is simply a particular orbit that is determined by a single point of the in-set I. The fact that Γ is a periodic orbit cannot be deduced from the flowbox alone. Rather, one needs to take into account the global return R from O back to I, which is a contraction mapping

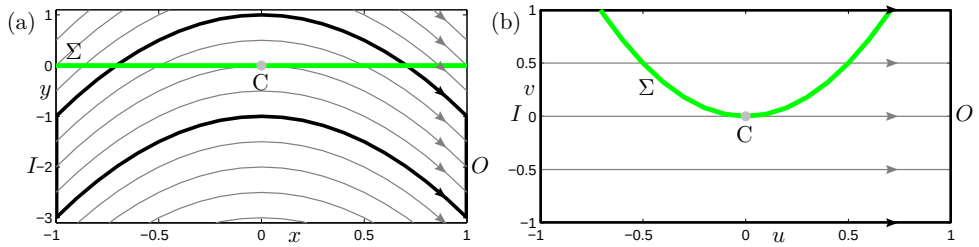

FIG. 5. *A straight section in a quadratic flow (a) is conjugate to a parabolic section in the standard flowbox (b); in both cases the tangency locus is a single point.*

since Γ is an attracting orbit. In figure 4 the image $R(O)$ of the out-set is the thick brown segment on the in-set I.

The idea is now to consider only the flow inside the flowbox of figure 4. For $s = 1.7518$ the section Σ_s intersects Γ in the two points γ_0 and γ_1, as for the case $s = 1$ of section 3.1. Orbits inside the flowbox that are sufficiently close to Γ intersect Σ_s twice, but orbits below the tangency point C in the flowbox do not intersect Σ_s at all. For $s = s^* \approx 2.0670$ orbits above Γ intersect Σ_s, but orbits below Γ (that is, below the point C in the flowbox) do not. This is due to the non-transverse, quadratic tangency of Γ with Σ_{s^*}. Finally, for $s = 2.3822$ the periodic orbit Γ does not intersect the section Σ_s, so that points sufficiently close to Γ do not intersect Σ_s either. The overall situation concerning the periodic orbit Γ follows when one takes the map R from O to I into account. Namely, under repeated re-entry into the flowbox all orbits eventually intersect Σ_s infinitely often for $s < s^*$, while all orbits eventually do not return to Σ_s for $s > s^*$. We stress that this division is determined locally inside the flowbox by the quadratic tangency between Γ and Σ_s at $s^* \approx 2.0670$.

3.2. Normal form of the quadratic tangency bifurcation. Generically, the flow of a two-dimensional vector field may have a quadratic tangency at an isolated point of a given section Σ [34]. An example is the flow of the Van der Pol system (3.1) in figure 2. In other words, when one zooms in more and more near a tangency point, the flow looks more and more like a quadratic flow. To be specific, consider the quadratic flow

$$\left\{ \begin{array}{rcl} \dot{x} &=& 1, \\ \dot{y} &=& -2\,x \end{array} \right. \tag{3.3}$$

and the section $\Sigma = \{y = 0\}$. The situation is sketched in figure 5(a), where an associated flowbox is highlighted. The flow of (3.3) has a quadratic tangency with Σ at the origin, so that $C = \{0\}$. Note that this phase portrait (where $M = \emptyset$) is structurally stable. The flow in the flowbox of figure 5(a) is mapped to the standard flowbox (2.7) for $n = 2$ by the coordinate transformation

$$(u, v) = (x, x^2 + y). \tag{3.4}$$

In the process the straight section in (x, y)-space is mapped to parabolic sections in the (u, v)-space of the standard flowbox, so that we again have $C = \{0\}$; see figure 5(b).

PROPOSITION 3.1. *In any sufficiently small flowbox, the phase portrait near a quadratic tangency of an orbit of a flow in* $\mathbb{R}^2$ *with a Poincaré section is topologically*

equivalent to the phase portrait in the standard flowbox (2.7) for $n = 2$ given by the section

$$\Sigma = \{(u, v) \mid v = 2\,u^2\}. \tag{3.5}$$

The proof of Proposition 3.1 can be found in [34] for the related situation of a flow on a two-dimensional manifold with boundary. Note that singularity theory guarantees that there is a smooth map that maps the section and the tangent orbit to the standard flowbox as stated. What needs to be shown in addition is that this map can be chosen in such a way that orbits map to orbits. For completeness, we present the basic construction.

Proof. According to the Flowbox Theorem [27] there is a smooth coordinate transformation that maps the flow into the standard flowbox (2.7) for $n = 2$. Let $\widetilde{\Sigma}$ be the image of the section under this map. Without loss of generality we may assume that the tangent orbit is mapped to the flowline $\{v = 0\}$, the tangency point is at the origin, and $\widetilde{\Sigma}$ lies in the region where $v \geq 0$. Because the tangency is quadratic, $\widetilde{\Sigma}$ has (locally) exactly two intersections with each flowline for $v > 0$, namely one for $u < 0$ and one for $u > 0$. Then there is a smooth v-dependent coordinate change of u that 'slides' these two branches to the standard section Σ given by (3.5). A u-dependent rescaling of time then ensures that $\dot{u} = 1$. □

The local dynamics within the standard two-dimensional flowbox, that is, for $(u, v) \in [-1, 1]^2$, can be described by giving the transfer map ρ_I from the in-set I to the section Σ, the transfer map ρ_Σ from Σ to itself, and the transfer map ρ_O from Σ to the out-set O. Since not all orbits hit Σ, the map ρ_I is not everywhere defined; similarly, ρ_Σ is not defined for points that have no local returns to Σ. We have the following explicit formulae:

$$\begin{aligned}
u = \rho_I(v) &= \begin{cases} -\sqrt{v/2} & \text{for } \ 0 \leq v \leq 1, \\ \text{undefined} & \text{for } \ -1 \leq v < 0. \end{cases} \\
\rho_\Sigma(u) &= \begin{cases} -u & \text{for } \ -1 \leq u \leq 0, \\ \text{undefined} & \text{for } 0 < u \leq 1, \end{cases} \\
v = \rho_O(u) &= \begin{cases} 2u^2 & \text{for } 0 \leq u \leq 1 \\ \text{undefined} & \text{for } \ -1 \leq u < 0. \end{cases}
\end{aligned} \tag{3.6}$$

Similarly, the associated transfer times are

$$\begin{aligned}
\tau_I(v) &= 1 - \sqrt{v/2} \quad \text{for } 0 \leq v \leq 1, \\
\tau_\Sigma(u) &= \quad 2u \qquad \text{for } \ -1 \leq u \leq 0, \\
\tau_O(v) &= \ 1 - 2u^2 \quad \text{for } 0 \leq u \leq 1.
\end{aligned} \tag{3.7}$$

For a general flow with quadratic tangency (3.6) and (3.7) can be seen as normal forms that give the leading-order components of the respective transfer maps.

The singularities of the above transfer maps expose the local dynamics within the flowbox. Notice that ρ_I has a quadratic singularity at $v = 0$ due to the grazing of the trajectory at the minimum of the parabolic section Σ, that is, at C. Inside the standard flowbox the first-return map P is given for $-1 \leq u \leq 0$ as $P = \rho_\Sigma$. Clearly, the associated transfer time $\tau_\Sigma(u)$ goes to 0 as $u \to 0$. This corresponds to the fact that the quadratic tangency inside the flowbox gives rise to a discontinuity of P at C, as was discussed in section 3.1. The first-return map P on the part of Σ for $u > 0$

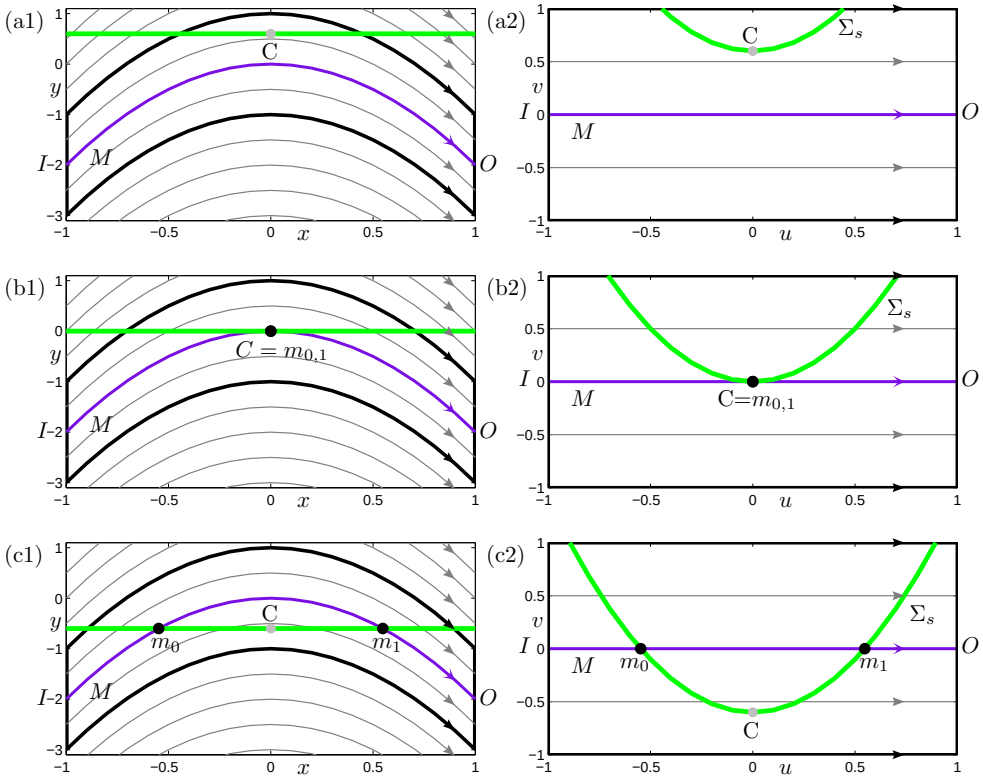

FIG. 6. *Unfolding of a quadratic tangency of an invariant manifold M (purple) with a Poincaré section (green). Shown are straight sections in a quadratic flow (left column), and the family of parabolic sections Σ_s in the standard flowbox (right column) for $s = 0.6$ (a), $s = 0$ (b), and $s = -0.6$ (c).*

inside the standard flowbox can only be defined if there exists a global return from the out-section O back to the in-section I in the form of a global return map R. If this is the case then we have $P = \rho_\Sigma \circ \rho_I \circ R \circ \rho_O(u)$ for $0 < u \leq 1$. As will be discussed in section 3.3, the existence of a global return R cannot be decided from information inside a flowbox; rather it depends on the global properties of the flow.

We now consider the case that the flowbox contains a one-dimensional invariant manifold that has a quadratic tangent with a particular section, as was the case for the Van de Pol system in figure 4. This *quadratic tangency bifurcation* is of codimension one, where we require the standard genericity condition that the dependence on the parameter is smooth and that the manifold crosses the section with positive speed. We have the following normal form result.

PROPOSITION 3.2. *In any sufficiently small flowbox, the unfolding of a generic quadratic tangency of a one-dimensional invariant manifold of a flow in $\mathbb{R}^2$ with a Poincaré section is topologically equivalent to the unfolding in the standard flowbox (2.7) for $n = 2$ given by the one-parameter family of sections*

$$\Sigma_s = \{(u, v + s) \mid v = 2\,u^2\}, \tag{3.8}$$

where the invariant manifold is the line

$$M = \{(u, v) \mid v = 0\}.$$

Proof. Suppose that the unfolding parameter of the quadratic tangency is η and the bifurcation takes place at $\eta = 0$. According to Proposition 3.1, any phase portrait of the unfolding in a flowbox near the quadratic tangency point is topologically equivalent to that given by $\widetilde{\Sigma} = \Sigma_0$ in the standard flowbox (2.7) for $n = 2$. Therefore, the invariant manifold (which is simply a single orbit) is mapped to a straight flowline $\widetilde{M} = \{v = s(\eta)\}$ in the standard flowbox, where $s(0) = 0$; furthermore, genericity of the dependence on η implies $\frac{ds}{d\eta}(0) \neq 0$, so that $s(\eta)$ unfolds the bifurcation. The result follows by applying the coordinate change $(u, v) \mapsto (u, v - s(\eta))$, which maps $\widetilde{M}$ to M and $\widetilde{\Sigma}$ to $\Sigma_{-s(\eta)}$. The thus constructed η-family of coordinate changes is continuous by the genericity assumption on η. □

Figure 6 illustrates the quadratic tangency bifurcation. The left column shows a flowbox of the quadratic flow (3.3) and a straight horizontal section. As was the case for figure 5, the coordinate transformation (3.4) relates the left column to the right column of figure 6, which illustrates Proposition 3.2 by showing the standard flowbox (2.7) with the parabolic section given by (3.8). In figure 6 row (a) shows the generic case $M \cap \Sigma_s = \emptyset$, row (b) is at the tangency where $M \cap \Sigma_s = C$ for $s = 0$, and row (c) is the generic case $M \cap \Sigma_s = \{m_0, m_1\}$. Note that the in-set I (that is, the v-space) acts as the parameter space, because the relative position of M and Σ_s is uniquely determined by $M \cap I$ relative to the projection of C onto I.

3.3. Global manifestations of a quadratic tangency. The example of a quadratic tangency bifurcation of the Van der Pol system as discussed in section 3.1 is a specific global manifestation of this bifurcation. Namely, the invariant manifold M of Proposition 3.2 is actually a segment of the attracting periodic orbit Γ. The intersection points $m_0 = \gamma_0$ and $m_1 = \gamma_1$ are fixed points of the Poincaré map, which can be defined on the whole of Σ when the global return R is taken into account. However, the invariant manifold M inside the flowbox does not need to be segment of a periodic orbit. Another generic and dynamically relevant situation is that M is a segment of a global stable or unstable manifold of an equilibrium. As an example, we consider the vector field

$$\left\{ \begin{array}{rcl} \dot{x} &=& y, \\ \dot{y} &=& \lambda y + x - x^2, \end{array} \right. \tag{3.9}$$

which was introduced in [17] as a system with a homoclinic bifurcation. We consider (3.9) for $\lambda = 0.25$ when the phase portrait is as in figure 7. The system has a saddle point at the origin with stable manifold $W^s(0)$ (blue) and unstable manifold $W^u(0)$ (red) as shown in figure 7. We consider a family of horizontal sections $\Sigma_s = \{(x, y) \mid y = s\}$ (green), which has a tangency with $W^u(0)$ for $s^* \approx 0.7669$. When one restricts attention to a suitable flowbox (boldface curves) then this tangency unfolds as described by the normal form in Proposition 3.2; compare with figure 6. However, the invariant manifold M inside the flowbox is now a segment of $W^u(0)$. Hence, points of the out-section O move off to infinity, so that they do not return to the in-section I; see figure 7. Hence, there exists no global return map R and the intersection points $m_0 = u_0$ and $m_1 = u_1$ do not correspond to fixed points of the first-return map P.

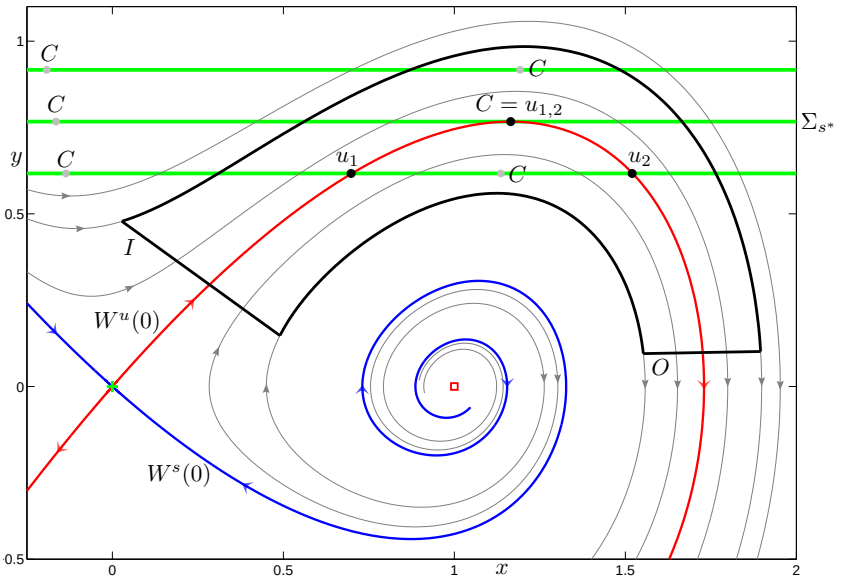

FIG. 7. *Phase portrait of the vector field (3.9) for* $\lambda = 0.25$ *with the stable manifold* $W^s(0)$ *(blue) and the unstable manifold* $W^u(0)$ *(red) of the origin. Also shown are three different choices of horizontal Poincaré section* Σ_s*, before, at and after a tangency of* $W^u(0)$ *with* Σ_s*, namely for* $s = 0.6169$*,* 0.7669 *and* 0.9169*, respectively. The black flowbox shows that this bifurcation unfolds as described by the normal form.*

Note that Teixera [34] considered the related situations that a periodic orbit or a separatrix interacts with the boundary of a two-dimensional flow. However, he treated these two global situations as different cases. By contrast, we take the point of view that the local bifurcation mechanism in a suitable flowbox is actually the same, while the overall meaning for the dynamics is determined by the exact nature of the invariant manifold that is involved in the tangency with the section (or boundary) inside the flowbox.

4. Quadratic tangency bifurcation in three-dimensional flows. An invariant manifold of a three-dimensional flow can be either one or two dimensional. Therefore, there are more possibilities for interactions of an invariant manifold with a two-dimensional section. As before, we discuss interactions in the context of a family of two-dimensional sections Σ_s at a regular point of the critical locus C, that is, at a generic tangency point between a three-dimensional flow and the section. To this end, we consider the standard flowbox (2.7) for $n = 3$, where we take $(v_1, v_2) = v \in [-1, 1]^2$ as coordinates. We start with a straightforward generalization of Proposition 3.2.

COROLLARY 4.1. *In a sufficiently small flowbox, the unfolding of a quadratic tangency of a one-dimensional invariant manifold of a flow in* $\mathbb{R}^3$ *with a global Poincaré section is topologically equivalent to the unfolding in the standard flowbox (2.7) for* $n = 3$ *given by the one-parameter family of sections*

$$\Sigma_s = \{(u, v_1, v_2 + s) \mid v_2 = 2\,u^2\}, \tag{4.1}$$

where the invariant manifold is line

$$M = \{(u, v) \mid (v_1, v_2) = (0, 0)\}.$$

Note that this bifurcation is of codimension one, because it involves the interaction of a one-dimensional manifold with a one-dimensional fold curve C in $\mathbb{R}^3$. In the standard flowbox the section Σ_s is a parabolic cylinder with the straight line $C = C(s) = \{(u, v_1, v_2 + s) \mid u = 0 \text{ and } v_2 = 0\}$ along which the flow has a quadratic tangency. This represents the generic situation inside a flowbox in the absence of cusp points on C, that is, in a sufficiently small neighborhood of a generic quadratic tangency point; see also [32, figure 5.1]. Note further that this unfolding reduces to the case for $n = 2$ of Proposition 3.2 by means of considering the two-dimensional slice for $v_1 = 0$. Therefore, the form of the transfer map ρ_I from the in-set I to the section Σ, the transfer map ρ_Σ from Σ to itself, and the transfer map ρ_O from Σ to the out-set O are as given in (3.6).

The new and more interesting possibility for $n = 3$ is the interaction of a two-dimensional invariant manifold M with a two-dimensional Poincaré section near a quadratic tangency of a single orbit. In this setting we do not consider the details of the dynamics on the part of M inside the flowbox, but simply consider M as a smooth family of one-dimensional orbit segments. To get some geometric insight, suppose that a quadratic tangency of M takes place in the standard flowbox for $n = 3$, where Σ is the parabolic cylinder given by (4.1). Then the invariant manifold is determined inside the flowbox by a smooth curve on the in-set I. If $M \cap I$ has a transverse intersection with the projection $\widehat{C} = \{v_2 = 0\}$ of C onto I, then this intersection and, hence, the quadratic tangency of the corresponding orbit is structurally stable and there is no bifurcation in the sense of Definition 2.3. However, we do get a bifurcation if $M \cap I$ has a tangency with $\{v_2 = 0\}$, which is generically quadratic. Note that there are two cases of quadratic tangency, depending on whether $M \cap I$ is curved up or curved down with respect to the (horizontal) projected fold curve $\widehat{C}$.

We say that there is a *codimension-one quadratic tangency bifurcation* between the two surfaces M and Σ at the point $\mathbf{x}^* = M \cap \Sigma$ if $M \cap I$ has a quadratic tangency with the projection (along flowlines) of C onto I. As a genericity condition we require that the dependence on the parameter is smooth and that M crosses Σ with positive speed. Note that this definition is general and does not depend on the choice of flowbox. The two cases of the quadratic tangency bifurcation are distinguished by whether $M \cap I$ lies in the region to which Σ projects or not, which we refer to as the *saddle case* and the *minimax case*, respectively.

PROPOSITION 4.2. *In any sufficiently small flowbox, the unfolding of a quadratic tangency of a two-dimensional invariant manifold of a flow in $\mathbb{R}^3$ with a Poincaré section is topologically equivalent to the unfolding in the standard flowbox (2.7) for $n = 3$ given by the one-parameter family of sections*

$$\Sigma_s = \{(u, v_1, v_2 + s) \mid v_2 = 2\,u^2 \pm 2\,v_1^2\} \tag{4.2}$$

where the invariant manifold is the plane

$$M = \{(u, v_1, v_2) \mid v_2 = 0\}.$$

The plus-sign in (4.2) gives the minimax case and the minus-sign the saddle case of the bifurcation.

Proof. Suppose that the unfolding parameter of the quadratic tangency is η and the bifurcation takes place at $\eta = 0$. In light of Corollary 4.1 we may consider a manifold $\widetilde{M}$ in the standard flowbox with $\Sigma_{s(\eta)}$ as given by (4.1), such that the quadratic tangency for $\eta = 0$ takes place at the origin. Then $\widetilde{M} \cap I$ is (locally and

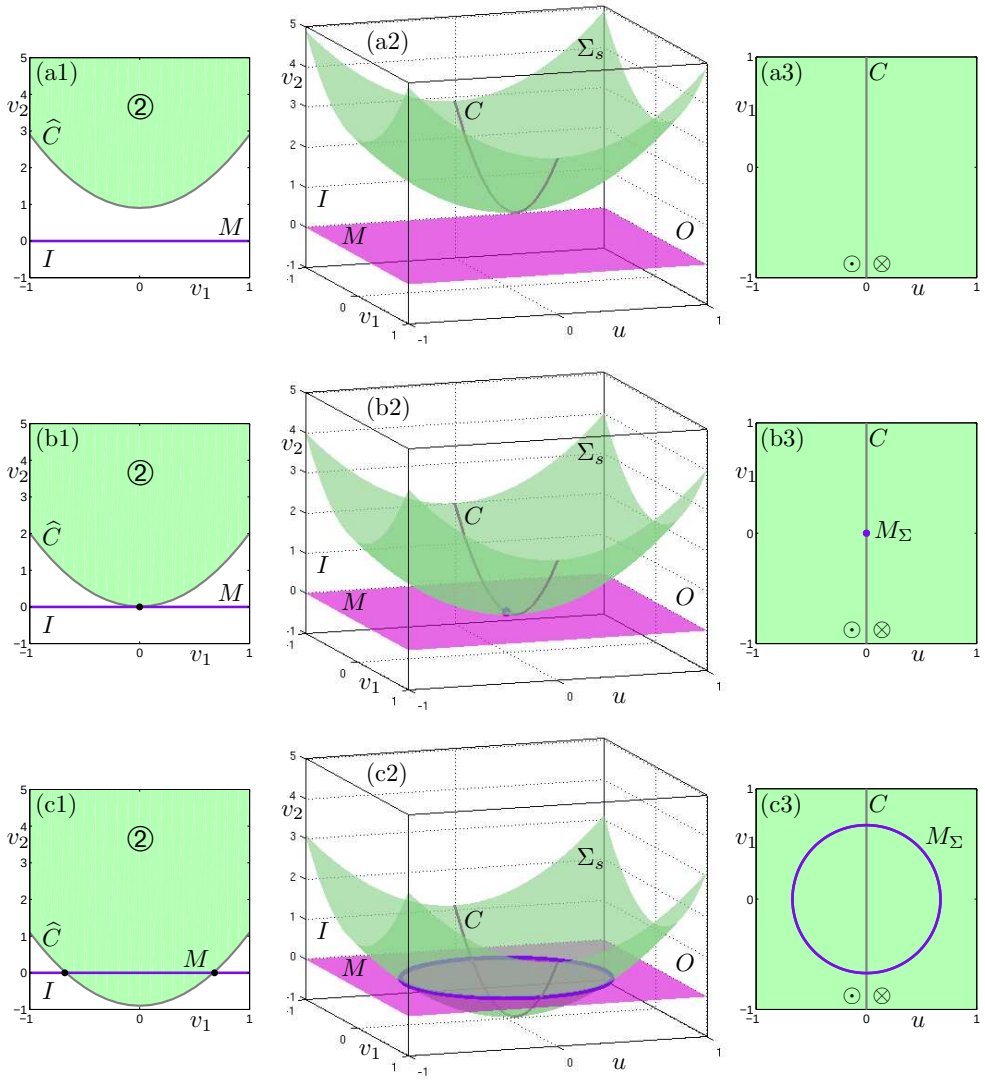

FIG. 8. *The minimax case of the quadratic tangency bifurcation, as described by the plus-sign in (4.2), before (a), at (b) and after (c) the bifurcation. The left column shows $M \cap I = \{v_2 = 0\}$ relative to the projection curve $\widehat{C}$ that bounds the projection of Σ_s (green region) onto the in-set I; the symbol ② indicates that there are two intersections with Σ in the green region. The middle column shows the section Σ_s (green) and the planar two-dimensional manifold M (pink); and the right column shows the intersection M_Σ in Σ_s. The tangency locus C (gray curve) separates the regions where the flow is upward ($\odot$) and downward ($\otimes$). Rows (a)–(c) are for $s = 0.9$, $s = 0.0$ and $s = -0.9$, respectively.*

for sufficiently small η) given by a function $\mu_\eta : v_1 \to v_2$ on the in-set I with a single minimum or maximum. Hence, the u-independent coordinate change $(u, v_1, v_2) \mapsto (u, v_1, v_2 - \mu_\eta(v_1) - s(\eta))$ maps $\widetilde{M}$ to the plane $\{v_2 = 0\}$. As a result, the image $\widetilde{\Sigma}_{s(\eta)}$ under this transformation is either a paraboloid or a saddle surface, where $s(\eta)$ is the v_2-value (vertical distance) of the maximum, the minimum, or the saddle point,

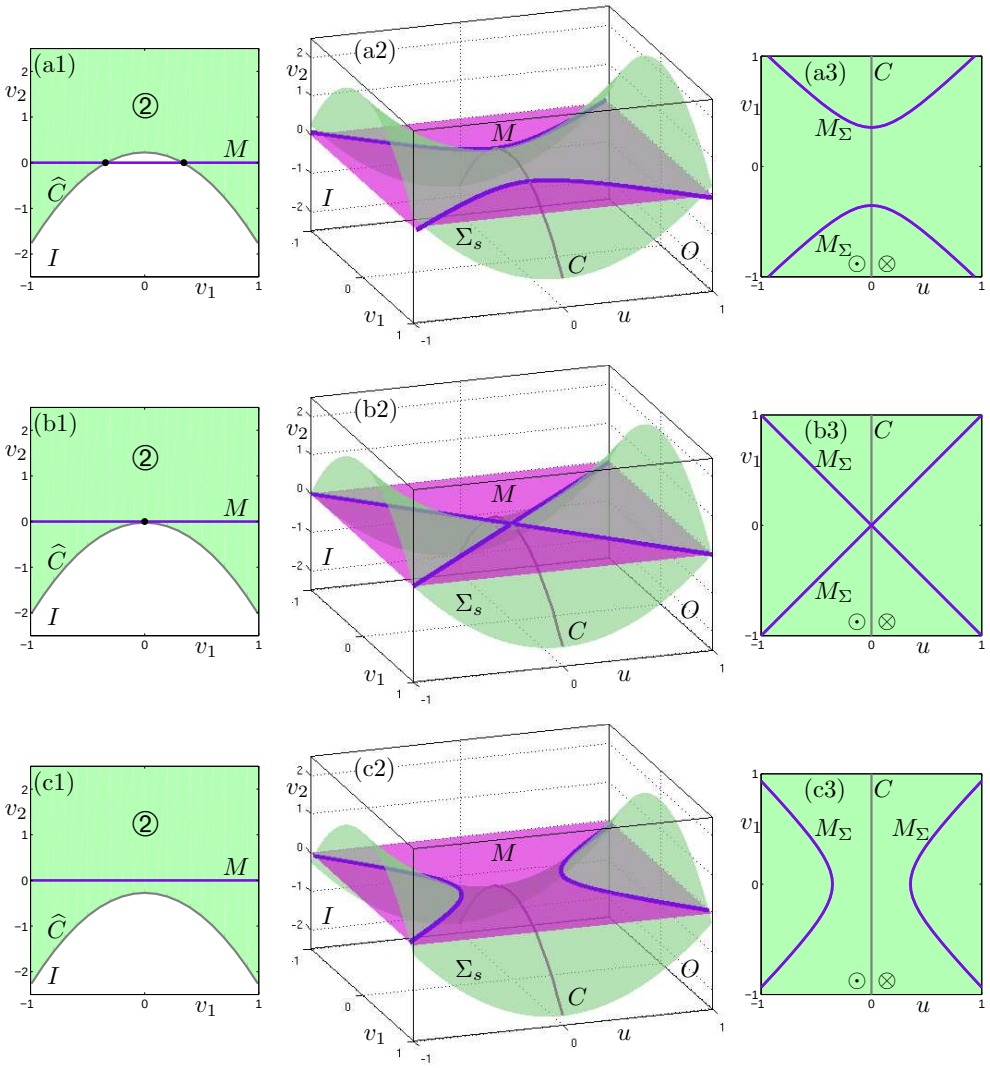

FIG. 9. *The saddle case of the quadratic tangency bifurcation, as described by the minus-sign in (4.2), before (a), at (b) and after (c) the bifurcation. The left column shows* $M \cap I = \{v_2 = 0\}$ *relative to the projection curve* $\widehat{C}$ *that bounds the projection of* Σ_s *(green region) onto the in-set* I*; the symbol ② indicates that there are two intersections with* Σ *in the green region. The middle column shows the section* Σ_s *(green) and the planar two-dimensional manifold* M *(pink), and the right column shows the intersection* M_Σ *in* Σ_s*. The tangency locus* C *(gray curve) separates the regions where the flow is upward (⊙) and downward (⊗). Rows (a)–(c) are for* $s = 0.25$*,* $s = 0.0$ *and* $s = -0.25$*, respectively.*

respectively. Therefore, for each η there exists a v_2-dependent coordinate change of v_1 that leaves the origin invariant, and a v_2-dependent coordinate change of u (as in the proof of Proposition 3.1) that together bring $\widetilde{\Sigma}_{s(\eta)}$ to the normal form given by (4.2). Again, a rescaling of time ensures that $\dot{u} = 1$. The thus constructed η-family of coordinate changes is continuous by the genericity assumption on η. □

From a singularity theory point of view, the two cases determined by the sign in (4.2) are the well-known transitions through a minimum or maximum (minimax for short), and through a saddle [2, 13, 38]. In particular, these are the only two generic cases and the unfolding given in Proposition 4.2 is versal.

The minimax and the saddle case of the quadratic tangency of Proposition 4.2 are illustrated in figures 8 and 9, respectively. In these figures the left-hand columns show the curve $M \cap I = \{v_2 = 0\}$ in the in-set I with the projection of Σ_s (green region) that is bounded by the projection $\widehat{C}$ of the fold curve C; any orbit in the green region intersects Σ twice in the flowbox. The middle columns show the section Σ_s (green) and the manifold M (pink) in the three-dimensional flowbox; the tangency locus C is the fold curve given by $u = 0$ in both cases. The right-hand columns show the corresponding intersections M_Σ (purple) in the Poincaré section Σ_s. The direction of the flow through Σ_s is indicated: the symbol $\odot$ denotes upward flow and the symbol $\otimes$ downward flow (with respect to the normal to the section). Rows (a) through (c) are before, at and after the respective bifurcations.

For the minimax transition in figure 8 the Poincaré section Σ_s is shown for $s = 0.9$ in row (a), $s = 0$ in row (b), and $s = -0.9$ in row (c). Row (a) shows no intersections between M and Σ_s. In row (b) the moment of minimax transition is shown, which is where M has an intersection with Σ_s at a single point that necessarily lies on the tangency locus C. Past the maximum transition M_Σ becomes a topological circle, as is shown in row (c). This circle is divided by C into two parts: points on the left half of M_Σ are mapped under the flow to the right half of M_Σ; the points on $M_\Sigma \cap C$ intersect Σ only once inside the flowbox. Note that the images of how the intersection M_Σ changes with the parameter s can be found in textbooks on singularity theory, such as [2, 13, 38]. However, the interpretation here is different as we also need to consider the action of the flow, as designated in figure 8 by the regions of upward (in the direction of increasing z, symbol $\odot$) and downward (in the direction of decreasing z, symbol $\otimes$) flow that are bounded by the tangency locus C.

The saddle transition is illustrated in figure 9 where Σ_s is shown for $s = 0.25$ in row (a), $s = 0$ in row (b), and $s = -0.25$ in row (c). Note that $M_\Sigma \neq \emptyset$ for all s. The intersection of M with Σ_s in row (a) consists of two arcs that both cross C. Points on each arc to the left of C return to Σ_s on the same arc to the right of C, namely, at the same value of v_1. The moment of the saddle transition is illustrated in row (b), where the two arcs of M_Σ meet on C to form a cross. In row (c) M_Σ consists of two arcs in a different way, namely, there is an arc in the region of upward flow and one arc in the region of downward flow; points on the left arc are mapped diffeomorphically to the right arc. Again, the action of the flow in the two different regions is an important element for the interpretation of the saddle transition in this context.

4.1. Intersection of an invariant two-torus with a plane. As for the case $n = 2$ in section 3.2, the question arises how the minimax and the saddle transitions in a flowbox manifest themselves for a given three-dimensional vector field. This depends again on whether there is a global return R from the two-dimensional out-set O back to the two-dimensional in-set I. The most natural setting in which such a global return may occur is that the segment M inside the flowbox is part of an invariant two-torus $\mathbb{T}$ of the underlying flow. In this case, the global return map R leaves M invariant, meaning that $M \cap O$ is mapped back to $M \cap I$. When the torus is attracting, R contracts the v_2 direction of the standard flowbox.

Indeed, the quadratic tangencies of section 4 all naturally occur in a three-dimensional vector field with an attracting invariant torus $\mathbb{T}$ that surrounds a periodic

orbit Γ. Bifurcations of the Poincaré map on a section can be brought about either by changing the section or by changes to the torus. To show this, we first consider a simple geometric example that is given by the unit circle

$$\Gamma = \{(x,y,z) \in \mathbb{R}^3 \mid x = \cos\theta,\ y = 0,\ z = \sin\theta, \quad \text{where } 0 \le \theta < 2\pi\} \tag{4.3}$$

in the (x,z)-plane, surrounded by a tube of radius r that forms the torus

$$\begin{aligned}\mathbb{T} = \{(x,y,z) \in \mathbb{R}^3 \mid\ & x = (1 + r\cos\phi)\cos\theta,\ y = r\sin\phi,\\ & z = (1 + r\cos\phi)\sin\theta, \quad \text{where } 0 \le \theta, \phi < 2\pi\}.\end{aligned} \tag{4.4}$$

We may consider $\mathbb{T}$ and Γ as a geometric model of an invariant torus surrounding a periodic orbit of an unspecified vector field, as long as $\mathbb{T}$ does not have self-intersections, that is, for $0 < r < 1$. We now consider the family of global planar Poincaré sections $\Sigma_s = \{(x,y,z) \in \mathbb{R}^3 \mid z = s\}$. While we are not specifying an underlying flow, we make the assumption that the tangency locus $C \subset \Sigma_s$ is given by the condition $x = 0$; note that this is consistent with the desired invariance of $\mathbb{T}$ and Γ. For specificity we further assume that the flow is upward ($\odot$) on Σ_s for $x < 0$ and downward ($\otimes$) for $x > 0$.

We first consider the scenario where $r = 0.5$ is fixed and s varies, that is, Γ and $\mathbb{T}$ are fixed invariant objects and Σ_s changes with the parameter s; this is illustrated in figure 10 in (x,y,z)-space, while figure 11 shows the invariant objects in the planar section Σ_s. The intersection $\mathbb{T}_\Sigma$ of the torus $\mathbb{T}$ (pink) and the section Σ_s (green) is highlighted in purple in each panel of figure 10, and the intersection points Γ_Σ of Γ (black) and Σ_s are marked with black dots. As before, the direction of the flow through Σ_s is indicated by the symbols $\odot$ (upwards) and $\otimes$ (downwards).

Figures 10 and 11 show the transition from $s = 0.45$ to $s = 1.6$; see also the accompanying animation jcko_a1.gif. Note that for the specific example of $\mathbb{T}$ as defined by (4.4) the family of intersection curves $\mathbb{T}_\Sigma$ comprise part of the family of Cassini ovals [25]; nevertheless, the qualitative nature of the transition shown here is what must be expected in general. For values $|s| < 0.5$ the intersection $\mathbb{T}_\Sigma$ consists of two disjoint closed curves centered around the intersection points $\gamma_0, \gamma_1 \in \Gamma_\Sigma$. For $s = 0$ we have that $\mathbb{T}_\Sigma$ consists of two circles of radius $r = 0.5$ centered around $\gamma_0, \gamma_1 = (\pm 1, 0, 0)$. In figures 10(a) and 11(a), where $s = 0.45$, these circles have become ovoid in nature, elongated towards C. Note that the points γ_0 and γ_1 also moved closer to C. This process continues until the first bifurcation of the Poincaré map at $s = 0.5$ is reached, where the two ovoids meet and form a lemniscate; see figures 10(b) and 11(b). Locally near C this is a saddle transition; compare panels (a)–(c) of figures 10 and 11 with figure 9. For $0.5 < s < 1.5$ the intersection $\mathbb{T}_\Sigma$ is a single closed curve that crosses the tangency locus C. Figures 10(c) and 11(c) show the case $s = 0.55$, where $\mathbb{T}_\Sigma$ is a single oval narrowed at C, this narrowing decreases as s increases further and $\mathbb{T}_\Sigma$ becomes smaller, as is illustrated in figures 10(d) and 11(d) for $s = 0.9$. The next bifurcation occurs for $s = 1.0$ in panel (e), where the two intersection points γ_0 and γ_1 come together and disappear at the quadratic tangency between Γ and Σ_s; compare panels (d)–(f) of figures 10 and 11 with figure 6. For $s > 1.0$ the periodic orbit no longer intersects Σ_s and $\Gamma_\Sigma = \emptyset$, so that the closed curve $\mathbb{T}_\Sigma$ is the only invariant object left. The intersection $\mathbb{T}_\Sigma$ continues to shrink until it is a single point at a maximum transition that takes place at $s = 1.5$; compare panels (f)–(h) of figures 10 and 11 with figure 8. For higher values of s the torus $\mathbb{T}$ no longer intersects Σ_s; see figures 10(h) and 11(h).

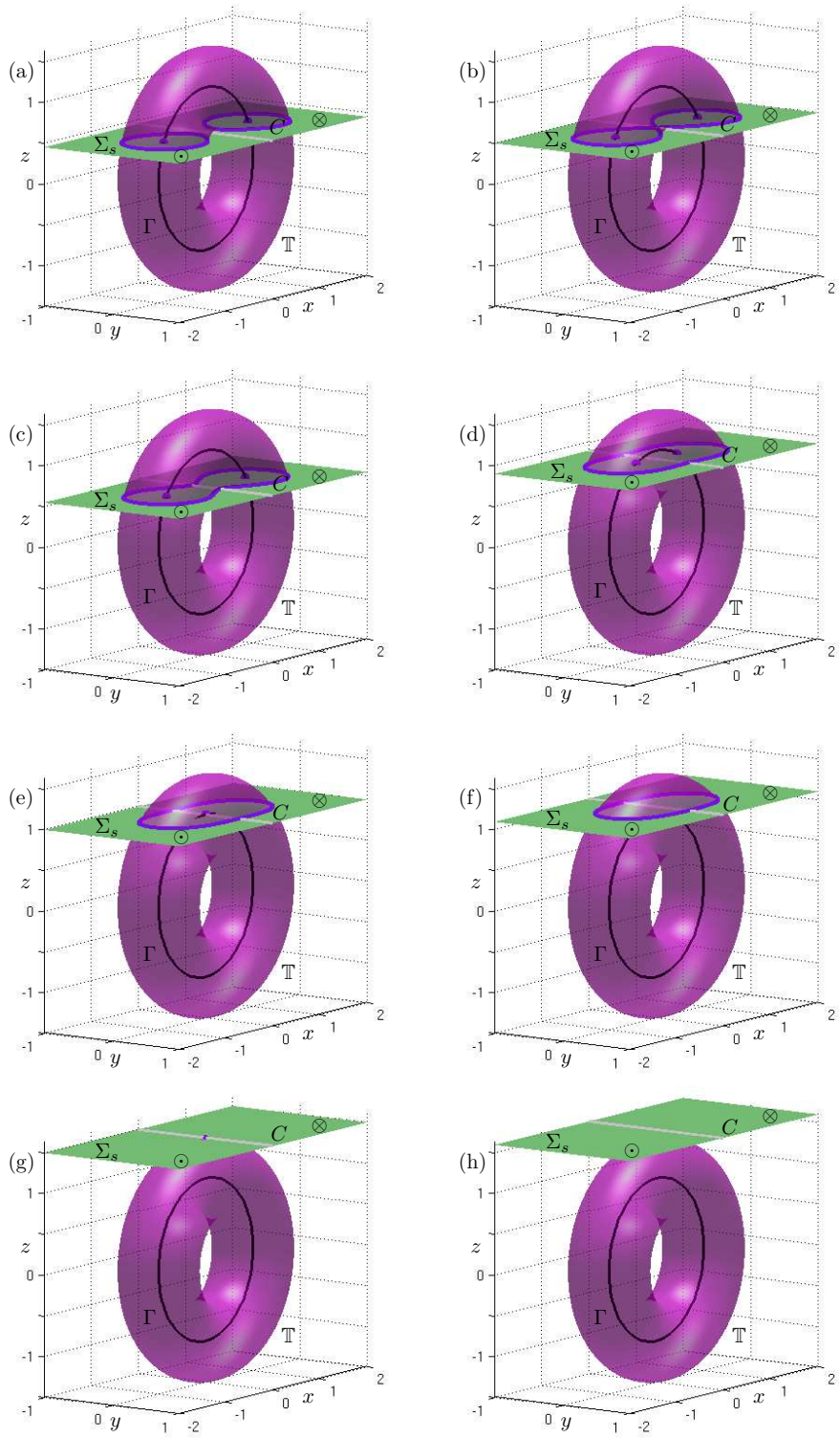

FIG. 10. *The geometric example (4.3)–(4.4) of a periodic orbit* Γ *(black curve) surrounded by an invariant torus* $\mathbb{T}$ *(pink) with radius* $r = 0.5$ *that are intersected by a planar Poincaré section* Σ_s *(green); the intersections* $\mathbb{T}_\Sigma = \mathbb{T} \cap \Sigma_s$ *are shown in purple and* $\Gamma \cap \Sigma_s$ *is indicated by black dots. Along* C *the flow is tangent to* Σ*, and the symbols* $\odot$ *and* $\otimes$ *indicate where the flow is upward and downward, respectively. From (a)–(h) the parameter* s *takes the values* 0.45, 0.5, 0.55, 0.9, 1.0, 1.1, 1.5, *and* 1.6*; see also figure 11 and animation jcko_a1.gif.*

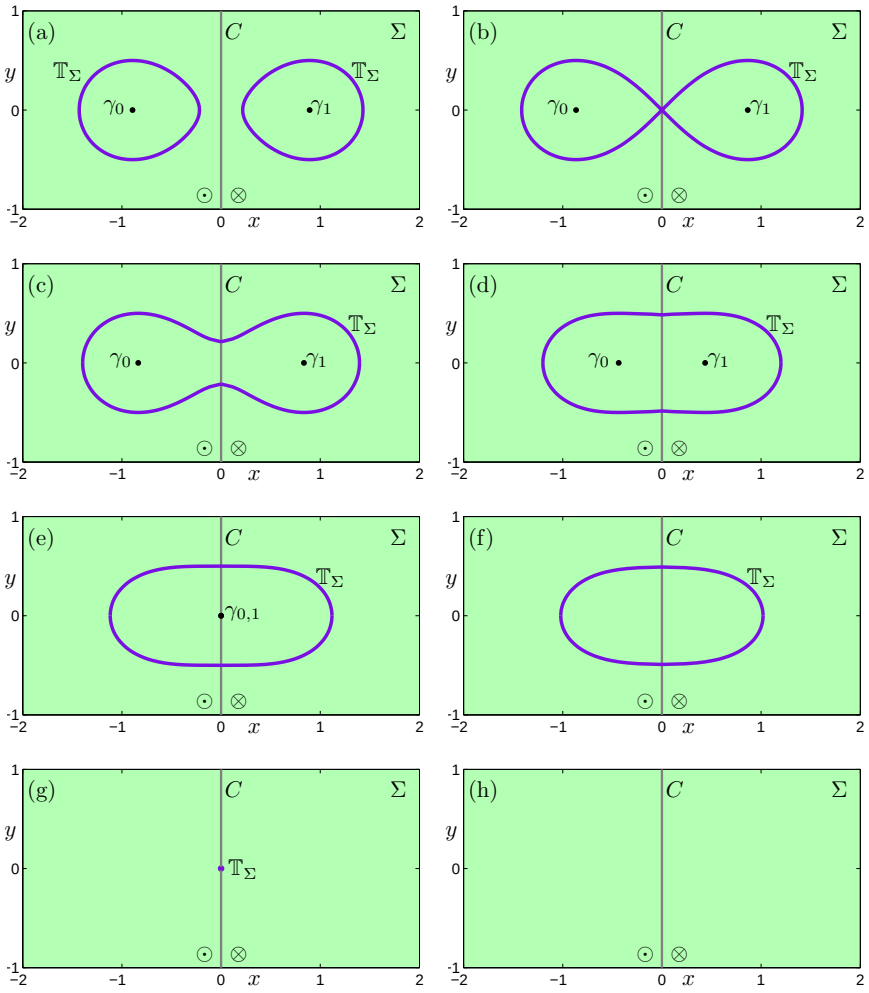

FIG. 11. *The intersections $\mathbb{T}_\Sigma$ and Γ_Σ in the section Σ_s. Along C the flow is tangent to Σ, and the symbols $\odot$ and $\otimes$ indicate where the flow is upward and downward, respectively. From (a)–(h) the parameter s takes the values* 0.45, 0.5, 0.55, 0.9, 1.0, 1.1, 1.5, *and* 1.6*; see also figure 10 and animation jcko_a1.gif.*

Figure 12 illustrates that a saddle transition of an invariant manifold in a Poincaré section may also take place when the section remains fixed and the invariant torus changes its 'thickness'; see also the accompanying animation jcko_a2.gif. Specifically, we consider the intersection of the torus $\mathbb{T}$ for varying radius r with the fixed section $\Sigma_{0.5}$; the central periodic orbit Γ also remains fixed, so that its intersection $\Gamma_\Sigma = \{\gamma_0, \gamma_1\}$ does not change. The r-dependent family of intersection curves $\mathbb{T}_\Sigma$ again comprise part of the family of Cassini ovals. For values of $r < 0.5$ the intersection $\mathbb{T}_\Sigma$ consists of two disjoint curves. For small r these curves are two circles centered around γ_0 and γ_1. As r increases these (topological) circles become more ovoid in nature, again elongating towards C; see row (a) of figure 12 for $r = 0.4$. As before, the two ovoids touch and form a lemniscate at $r = 0.5$, which is illustrated in row (b) of figure 12. For $0.5 < r < 1.0$ the intersection $\mathbb{T}_\Sigma$ is a single closed curve, as is shown

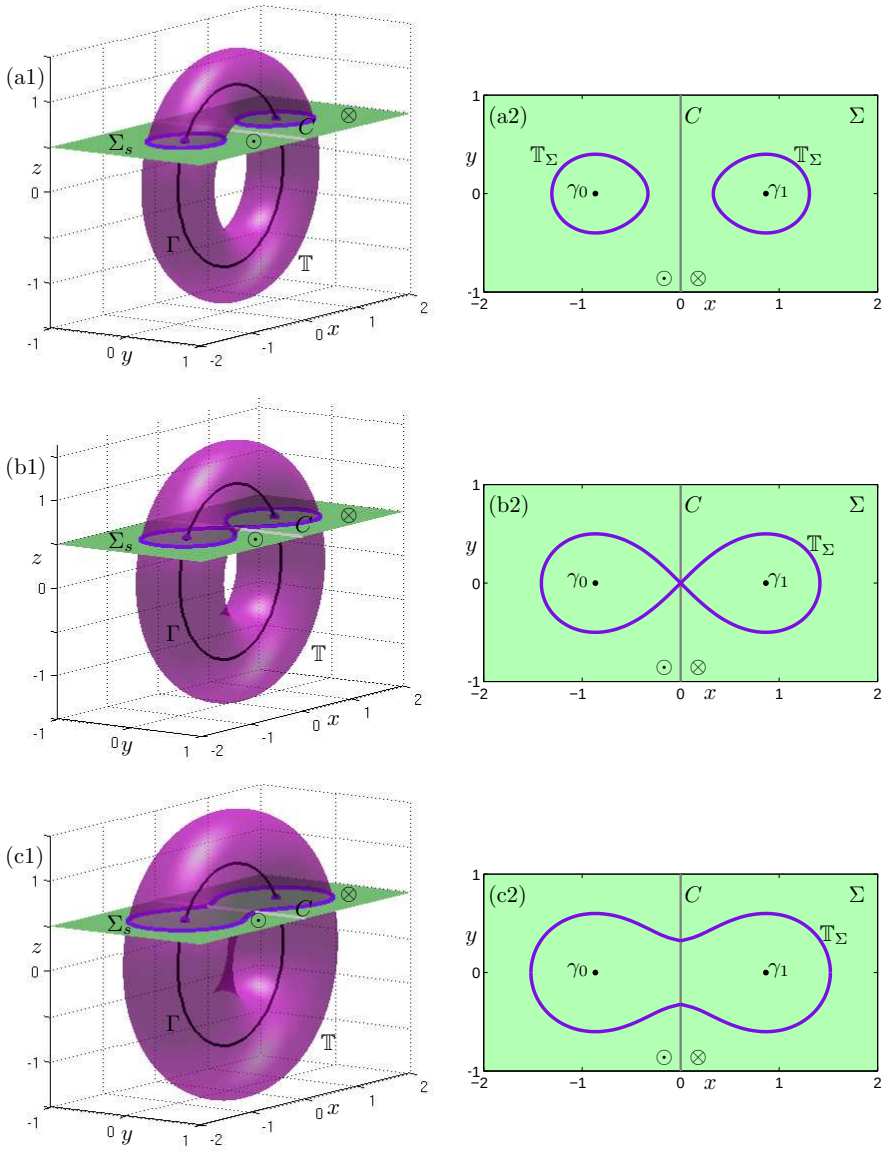

FIG. 12. *The geometric example (4.3)–(4.4) of a periodic orbit* Γ *surrounded by an invariant torus* $\mathbb{T}$ *(pink) of varying radius* r *that are intersected by the fixed planar Poincaré section* Σ_s *(green) for* $s = 0.5$*. The left column shows the situation in* (x, y, z)*-space, and the right column shows* $\mathbb{T}_\Sigma$ *and* $\Gamma_\Sigma = \{\gamma_0, \gamma_1\}$*; along* C *the flow is tangent to* Σ*, and the symbols* $\odot$ *and* $\otimes$ *indicate where the flow is upward and downward, respectively. In rows (a)–(c) the radius* r *takes the values* 0.4, 0.5 *and* 0.6*; see also animation jcko_a2.gif.*

in row (c) for $r = 0.6$. For increasing $r > 0.5$ the curve $\mathbb{T}_\Sigma$ gradually transforms into an oval. Clearly, the bifurcation, locally near C, is a saddle transition as described by Proposition 4.2; compare figure 12 with figure 9. Note that it is possible to have a minimax transition by varying the radius of the torus, but then a different choice

of section must be made; an example would be $\Sigma_{1.5}$ with a change of the radius of $\mathbb{T}$ through $r = 0.5$.

4.2. Saddle transitions in a semiconductor laser system. To demonstrate how quadratic tangencies arise in a practical example, we consider the model of a semiconductor laser with optical injection given by the equations

$$\left\{ \begin{array}{rcl} \dot{E} & = & K + \left(\frac{1}{2}\left(1 + i\alpha\right) n - i\omega\right) E, \\ \dot{n} & = & -2\gamma n - \left(1 + 2Bn\right)\left(|E|^2 - 1\right), \end{array} \right. \tag{4.5}$$

where $E = E_x + iE_y$ is the complex electric field and n is the population inversion. The parameters α, B, and γ characterise the material properties of the laser, ω is the detuning, and K the injection field strength; see [36] for further details. In this paper $\alpha = 2$, $B = 0.015$, $\gamma = 0.035$ and $\omega = 0.43$ are used throughout, while K is varied.

As was done in [36], we choose the fixed Poincaré section

$$\Sigma = \{(E, n) \in \mathbb{C} \times \mathbb{R} \mid n = -0.1\}. \tag{4.6}$$

By numerical integration of (4.5) it can be found quite easily that, for a range of the injection strength K around 0.1139, the Poincaré map on Σ shows attracting invariant curves surrounding points of an unstable period-six orbit $\{\gamma_0, \ldots \gamma_5\}$; see figure 13. As can be seen from the panels of this figure, the number of invariant curves, labeled $\mathbb{T}_\Sigma$, changes with K.

One might be tempted to think that the change in the number of invariant curves is due to a bifurcation of the vector field (4.5), but this is not the case. Instead, there are several saddle transitions involving an underlying attracting invariant torus $\mathbb{T}$; see figure 14. The torus $\mathbb{T}$ has been obtained by integrating from a suitable initial condition (after omitting transients), because the dynamics on it appears to be quasi-periodic (or of very high period); figure 14 shows $\mathbb{T}$ (mauve) computed as a single orbit over 60,000 time steps of size 0.01; the repelling periodic orbit Γ inside $\mathbb{T}$ is also shown; it was found as a fixed point of the sixth return map to the Poincaré section Σ. Indeed, as is shown in figure 14, there are exactly six intersections of Γ (black) and Σ (green).

To compare with the theory, note that the flow of (4.5) is tangent to Σ along the tangency locus

$$C = \left\{ (E, n) \in \Sigma \mid \ |E|^2 = \Delta(-0.1) \right\}, \tag{4.7}$$

where

$$\Delta(n) := 1 - \frac{2\gamma n}{1 + 2Bn}. \tag{4.8}$$

Hence, C is a circle in Σ that is centered at $(0, 0, -0.1)$ with radius $\sqrt{\Delta(n)} \approx 1.0035$ for the given system parameters. We conclude from equation (4.5) that the flow points in the positive n-direction ($\odot$) inside C, and in the negative n-direction ($\otimes$) outside C.

In figures 13 and 14 the parameter K is varied and related panels are for the same values of K. In panel (a) the intersection $\mathbb{T}_\Sigma$ consists of six disjoint invariant circles, each surrounding an intersection point γ_i. Under the first-return map P on Σ each invariant circle is mapped to another invariant circle in $\mathbb{T}_\Sigma$. Note that a circle outside

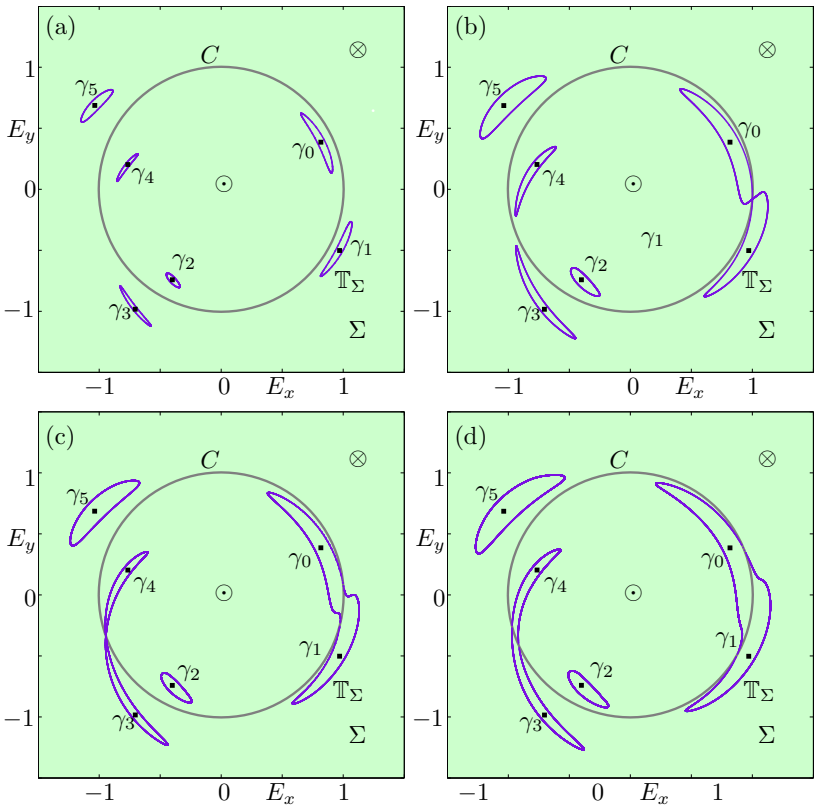

FIG. 13. *The Poincaré map of (4.5) in the fixed section* Σ *defined by (4.6) has a number of attracting invariant curves, labeled* $\mathbb{T}_\Sigma$*, that surround points of an unstable period-six orbit* $\Gamma_\Sigma = \{\gamma_0, \ldots \gamma_5\}$*. The number of invariant curves in* $\mathbb{T}_\Sigma$ *depends on the value of the injection strength* K*. Also shown is the circular tangency locus* C *given by (4.7) that divides* Σ *into two regions with upwards (⊙) and downward (⊗) flow. From (a)–(d)* K *takes the values* 0.1139, 0.11392468, 0.1139281, *and* 0.11395*; compare with figure 14.*

C is mapped to one inside C, and vice versa. A neighborhood of each consecutive pair is topologically equivalent to figure 12(a). Panel (b) of figures 13 and 14 shows the first saddle transitions, where the invariant circles around γ_0 and γ_1 join to form a single invariant circle; locally the situation is topologically equivalent to figures 12(b) and 9(b). While each component of $\mathbb{T}_\Sigma$ in figure 13(a) maps to itself under the sixth return of P, this is no longer true after the saddle transition in figure 13(b). After the bifurcation, as shown in figure 13(c), the part inside C of the large component of $\mathbb{T}_\Sigma$ that surrounds γ_0 and γ_1 is mapped under P to the part of the same component that lies outside C. On the other hand, the outside part of this component is mapped under P^5 back to the inside part. Note that panel (c) of figures 13 and 14 also show the next saddle transition of the two invariant circles surrounding γ_3 and γ_4. Panel (d) of figures 13 and 14 shows the situation after the second saddle-transition with the set of four circles in Σ that is invariant under P; two of the invariant circles now surround a pair of points of Γ_Σ.

As can be seen from the three-dimensional images of figure 14, the invariant torus $\mathbb{T}$ does not appear to undergo any bifurcations (meaning that it remains a normally hyperbolic invariant manifold). The topological changes of the invariant set $\mathbb{T}_\Sigma$ of the

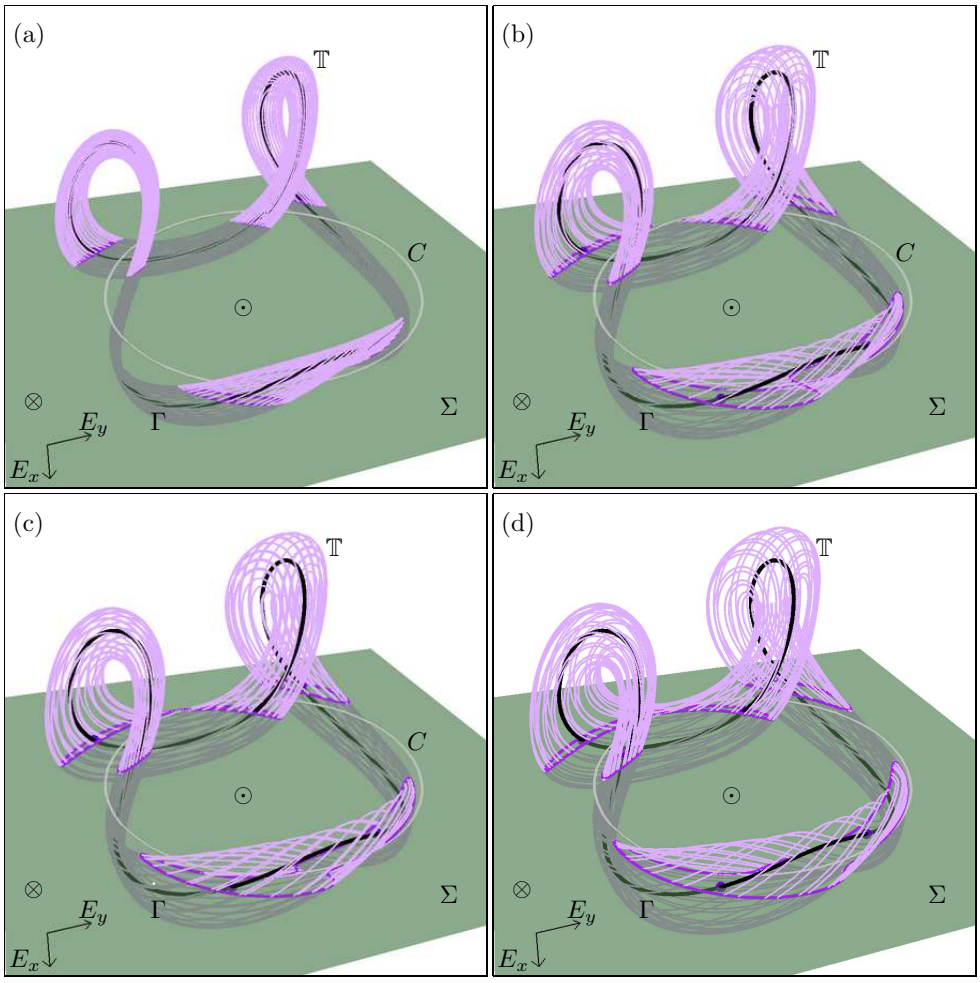

FIG. 14. *The sets* $\mathbb{T}_\Sigma$ *and* Γ_Σ *in figure 13 of the Poincaré map of (4.5) on the section* Σ *defined by (4.6) are intersections of an attracting invariant torus* $\mathbb{T}$ *and a repelling periodic orbit* Γ *of the flow. Also shown is the circular tangency locus* C *given by (4.7) that divides* Σ *into two regions with upwards (*$\odot$*) and downward (*$\otimes$*) flow. From (a)–(d)* K *takes the values* 0.1139, 0.11392468, 0.1139281, *and* 0.11395.

Poincaré map shown in figure 13 are entirely due to the fact that the torus changes its 'thickness' with the injection strength K, which leads to saddle transitions. This is exactly the mechanism that was demonstrated with the simple geometric example in figure 12. Our investigation of the laser system shows that tangency bifurcations of an invariant manifold with a two-dimensional section must indeed be expected in concrete applications, even when the Poincaré section is kept fixed. Indeed, it is quite natural that invariant objects, such as periodic orbits and invariant tori, change their size and/or shape upon variation of a system parameter. As we have seen, changing a single parameter may lead to several topological changes of invariant sets in the Poincaré section.

5. Cubic tangency bifurcation in three-dimensional flows. In this section we discuss a different and final codimension-one tangency bifurcation of a two-dimensional invariant manifold of a three-dimensional flows. We identify and characterize this bifurcation in a planar section in the semiconductor laser system equation (4.5) in the next section. We then discuss the geometry with a simpler geometric model in section 5.2, and finally derive the normal form in section 5.3.

However, first we introduce a new geometric object — the *extended critical locus* denoted $\mathcal{C}$ — to help understand the geometry of the flow. Suppose that we have as part of the setup a one-parameter family Σ_s of sections such that the bifurcation occurs at $\mathbf{x}^* \in \Sigma_{s^*}$. (If, as in the laser system, we are starting with only a single section Σ then we define the family Σ_s in a natural way by moving it in the direction of the unit normal vector $\vec{n}_\Sigma(\mathbf{x})$, formally $\Sigma_s = \{\mathbf{x} + s\,\vec{n}_\Sigma(\mathbf{x}) \mid \mathbf{x} \in \Sigma\}$ and $\Sigma = \Sigma_{s^*}$; note that for sufficiently small s each Σ_s is a global Poincaré section in the sense of (2.4).) The extended critical locus $\mathcal{C}$ is now defined as the union of the critical tangency loci $C(s)$ of the sections Σ_s, that is,

$$\mathcal{C} = \bigcup_s C(s). \tag{5.1}$$

We assume here that the dependence of Σ_s on s is smooth, so that $\mathcal{C}$ is a smooth codimension-one submanifold of the phase space $\mathbb{R}^n$. Therefore, $\mathcal{C}$ is of the same dimension as the section Σ (i.e., it is a surface for $n = 3$) and $\mathcal{C} \cap \Sigma = C$. Generically, the extended critical locus is transverse to Σ_s and, hence, knowing properties of the flow through $\mathcal{C}$ gives new geometric insight. We define the tangency locus D on $\mathcal{C}$ by

$$D := \{\mathbf{x} \in \mathcal{C} \mid f(\mathbf{x}) \cdot \vec{n}_{\mathcal{C}}(\mathbf{x}) = 0\}, \tag{5.2}$$

where $\vec{n}_{\mathcal{C}}(\mathbf{x})$ is the unit normal to $\mathcal{C}$ at the point $\mathbf{x}$. As with C on Σ the tangency locus D generically consists of codimension-one submanifolds (i.e., curves for $n = 3$) that divide $\mathcal{C}$ into regions with opposite directions of the flow.

5.1. Cubic tangency bifurcation in the semiconductor laser system. When the parameter K of the semiconductor laser system equation (4.5) is increased to values beyond those shown in figure 13 then one encounters the codimension-one bifurcation of the invariant torus $\mathbb{T}$ that is illustrated in figures 15 and 16.

Figure 15(a) is a three-dimensional image of the surfaces $\mathbb{T}$, Σ and $\mathcal{C}$ at the moment of bifurcation for $K \approx 0.1140145$. The extended tangency locus $\mathcal{C}$ was computed by considering the natural family of sections

$$\Sigma_s = \{(E, n) \in \mathbb{C} \times \mathbb{R} \mid n = s\}$$

where $\Sigma = \Sigma_{s^*}$ for $s^* = -0.1$. It follows from (4.7) and (4.8) that

$$\mathcal{C} = \left\{(E, n) \in \mathbb{C} \times \mathbb{R} \mid |E|^2 = \Delta(n)\right\}, \tag{5.3}$$

which is a cone. Furthermore, we find that

$$D = \left\{(E, n) \in \mathcal{C} \mid E_x = -\frac{n}{2K}\Delta(n),\ E_y = \sqrt{\Delta(n) - \frac{n^2}{4K^2}\Delta(n)^2}\right\}, \tag{5.4}$$

where n is chosen such that $E_y \in \mathbb{R}$, that is, $|n| \leq 2k/\sqrt{\Delta(n)}$. The cone $\mathcal{C}$ is the gray surface in figure 15(a) that is divided by D (closed white curve) into two parts. The

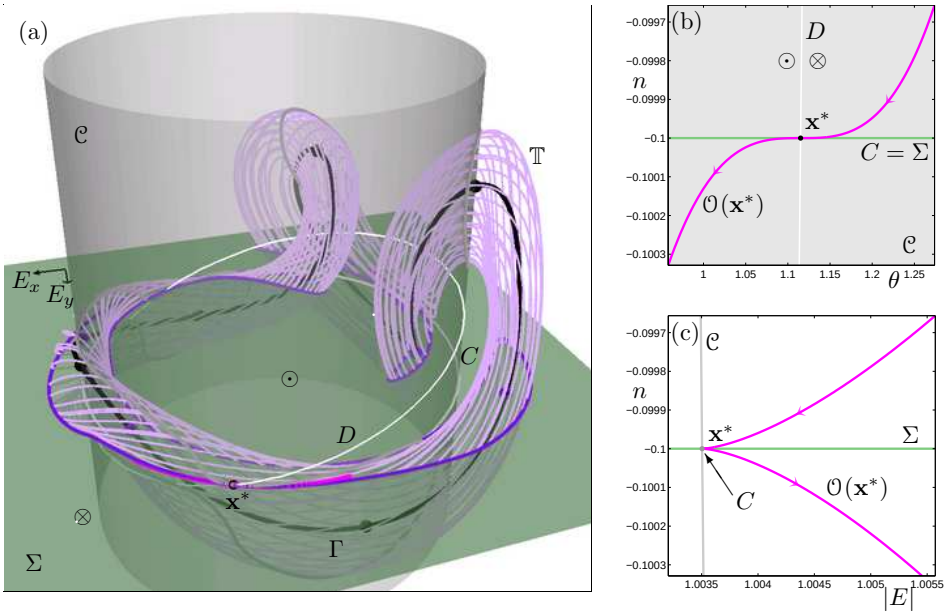

FIG. 15. *Panel (a) shows the invariant torus $\mathbb{T}$ (mauve) of (4.5) at the moment of the cubic tangency bifurcation at $\mathbf{x}^* \approx (0.44162, 0.90111, -0.1)$ for $K \approx 0.1140145$; compare with figure 16(b). Also shown are the section Σ (green), the extended critical locus $\mathcal{C}$ (gray) and the respective intersection curves with $\mathbb{T}$. A segment of the orbit $\mathcal{O}(\mathbf{x}^*)$ (magenta curve) is shown in panel (b) in the (θ, n)-plane, and in panel (c) in the $(|E|, n)$-plane (where $E = |E|e^{i\theta}$).*

flow points from the inside of $\mathcal{C}$ to the outside above D and from the outside of $\mathcal{C}$ to the inside below D.

At the moment of bifurcation, illustrated in figure 15, the torus $\mathbb{T}$ crosses the section Σ at the intersection point $\mathbf{x}^* \in C \cap D$ of C and D. Therefore, $\mathbb{T}_\Sigma$ is tangent to C in Σ and $\mathbb{T}_\mathcal{C}$ is tangent to D in $\mathcal{C}$; see row (b) of figure 16. The passage of a two-dimensional invariant manifold through a point $\mathbf{x}^* \in C \cap D$ could be used as the defining property of this codimension-one bifurcation. However, we prefer to characterize this phenomenon in terms of a property of the orbit $\mathcal{O}(\mathbf{x}^*) \subset M$. Figure 15(a) shows a relevant segment of $\mathcal{O}(\mathbf{x}^*)$ (magenta curve). Notice that this orbit segments remains very close to Σ and that it is very difficult to judge its position relative to other flow lines. Therefore, figure 15(b) and (c) show the orbit through $\mathbf{x}^*$ in the radial and angular projections of $E = |E|e^{i\theta}$, that is, in the (θ, n)-plane and in the $(|E|, n)$-plane, respectively. In these projections one can clearly see the determining property of this orbit: it has a cubic tangency with the section Σ at $\mathbf{x}^*$, which is why we refer to this bifurcation as the *codimension-one cubic tangency bifurcation.*

What happens when one moves through the cubic tangency bifurcation for $K \approx 0.1140145$ is illustrated in figure 16, where the green panels on the left show $\mathbb{T}_\Sigma$ in Σ and the gray panels on the left show $\mathbb{T}_\mathcal{C}$ in $\mathcal{C}$. Note that $\mathcal{C}$ has been 'unrolled' and is shown in the (θ, n)-plane. Also shown are enlargements near the bifurcation point in Σ (green sub-panel) and in $\mathcal{C}$ (gray sub-panel), respectively; here $\mathbb{T}_\Sigma$ is plotted relative to the curve C, which appears as a straight line in the green sub-panels. As is shown in the left column of figure 16 and the associated green sub-panels, the curve

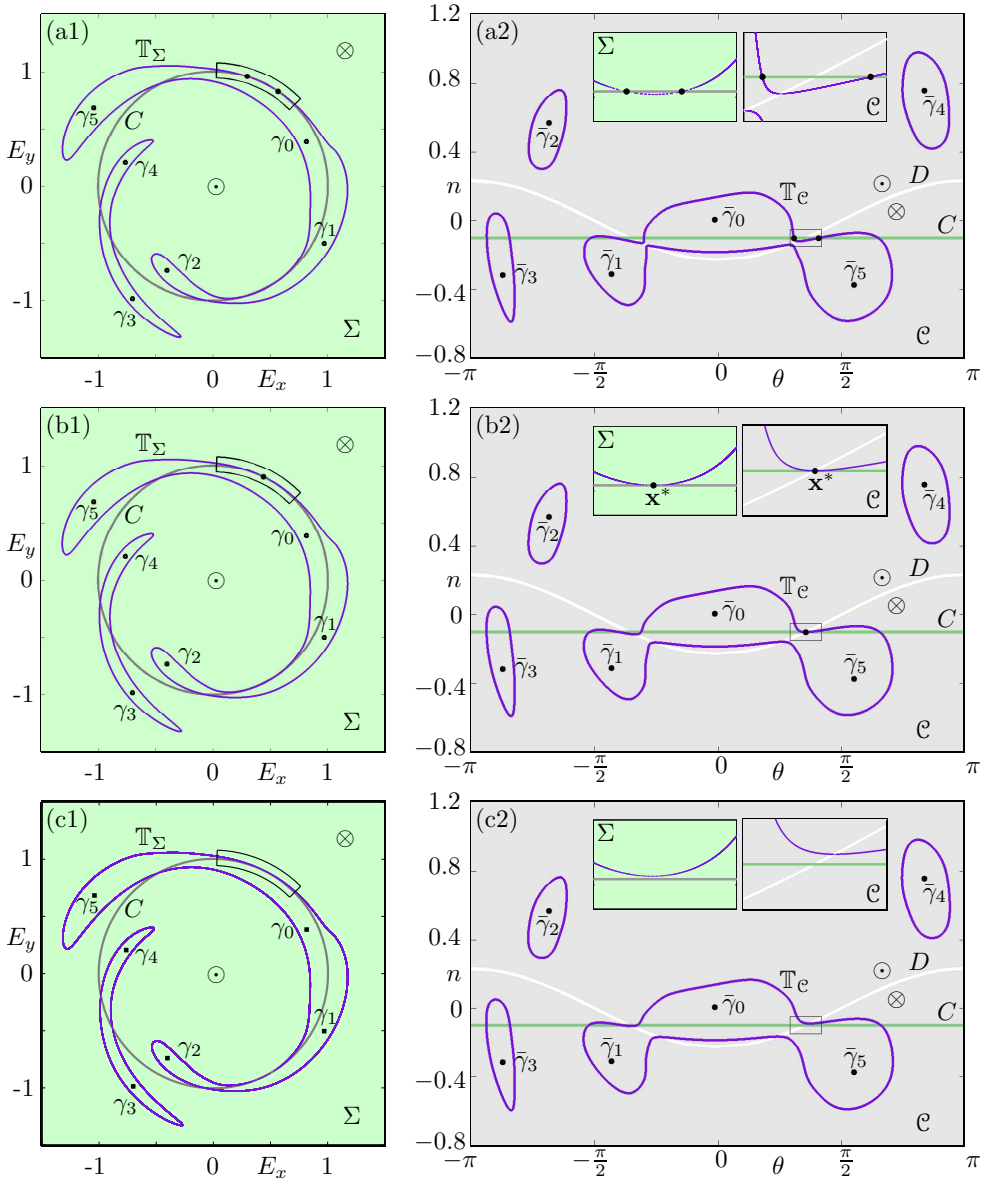

FIG. 16. *Cubic tangency bifurcation for (4.5). The three rows show the situation before, at and after the bifurcation. The left column shows the interaction of $\mathbb{T}_\Sigma$ with C in Σ, and the right column the interaction of $\mathbb{T}\mathcal{C}$ with D in $\mathcal{C}$; the sub-panels show enlargements near the tangency points in Σ (green sub-panel) and $\mathcal{C}$ (gray sub-panel) in the indicated regions. Rows (a)–(c) are for $K = 0.1140105, 0.1140145$ and 0.1140185, respectively; compare with figure 15(a).*

$\mathbb{T}_\Sigma$ moves relative to the curve C in the section Σ. At the same time we see in the right column of figure 16 and the associated gray sub-panels that $\mathbb{T}_\mathcal{C}$ moves relative to the curve $C = \Sigma \cap \mathcal{C}$ in the extended tangency locus $\mathcal{C}$. In figure 16(a) there are two intersections between $\mathbb{T}_\Sigma$ and C, and two between $\mathbb{T}_\mathcal{C}$ and C. Points on the part of $\mathbb{T}_\Sigma$ around γ_5 that lies outside C return to points on one of two separate arcs of $\mathbb{T}_\Sigma$, namely the large arc inside C near γ_0 or the small piece between the two intersection

points with C that is shown in the enlarged area of the Poincaré section. Figure 16(b) is at the moment of cubic tangency bifurcation when the invariant manifold $\mathbb{T}_\Sigma$ has a quadratic tangency with the tangency locus C at the point $\mathbf{x}^*$. At the same time $\mathbb{T}_\mathcal{C}$ has a quadratic tangency with C at $\mathbf{x}^*$. Even though this bifurcation of the Poincaré map does not change the invariant curve $\mathbb{T}_\Sigma$, it does make a difference to the dynamics on the Poincaré section, because it changes the number of segments of $\mathbb{T}_\Sigma$ on either side of the tangency locus C. After the bifurcation $\mathbb{T}_\Sigma$ and $\mathbb{T}_\mathcal{C}$ no longer intersect C; see figure 16(c). This means that now the part of $\mathbb{T}_\Sigma$ around γ_5 that lies outside C returns to a single arc of $\mathbb{T}_\Sigma$ inside C.

It is generally quite difficult to find orbits with cubic tangencies with a Poincaré section. Therefore, the insight that a cubic tangency bifurcation takes place when a two-dimensional invariant manifold $\mathbb{T}$ passes through a point in $C \cap D$ is very useful from a practical point of view. Namely, the set $C \cap D$ consists generically of isolated points that can be calculated analytically. In particular, a cubic tangency bifurcation can only occur when $C \cap D \neq \emptyset$. One readily computes that for $|n| \leq 2k/\sqrt{\Delta(n)}$ the curves D and C intersect in two points, which are given by

$$C \cap D = \left(\frac{0.1}{2K}\Delta(n),\ \pm\sqrt{\Delta_(n) - \frac{0.01}{4K^2}\Delta(n)^2},\ -0.1 \right) \approx \left(\frac{0.05035}{K}, \pm\frac{1}{2}\sqrt{4.02808 - \frac{0.01014}{K^2}}, -0.1 \right) \tag{5.5}$$

for the fixed values $\alpha = 2$, $B = 0.015$, $\gamma = 0.035$ and $\omega = 0.43$ used here, and for $s = s^* = -0.1$. Indeed for $\Sigma_{-0.1}$ there are exactly two points in $C \cap D$. At the bifurcation for $K \approx 0.1140145$ we have $C \cap D \approx \{(0.44162, \pm 0.90111, -0.1)\}$ and $\mathbb{T}$ crosses the point $\mathbf{x}^* \approx (0.44162, 0.90111, -0.1)$; see figures 15(a) and 16.

We finally remark that $C = D$ is not generic in our context, but it occurs stably in Hamiltonian vector fields. In fact, this geometric situation was identified (but not in terms of C and D) by Birkhoff [3] as the one that allows the construction of a complete Poincaré section. Namely, for $C = D$ the curve $C \in \Sigma$ is invariant under the flow and orbits are spiraling around C.

5.2. A helical tube with a cubic tangency bifurcation. It is quite clear from the previous section that a cubic tangency bifurcation involves an element of rotation of the flow around the curve C. To get geometric insight into how this bifurcation can be 'straightened out' to a normal form in the standard flowbox, we now consider a concrete geometric model of a cubic tangency bifurcation in a simplified curved flow; this model is in the spirit of the examples in section 4.1. As a 'framework' we consider

$$\Sigma_s = \{(x, y, z) \in \mathbb{R}^3 \mid z = s\} \tag{5.6}$$

in $\mathbb{R}^3$, where we assume further that the flow is such that

$$C = C(s) = \{(x, y, s) \in \Sigma_0 \mid y = 0\} \tag{5.7}$$

so that the flow points up for $y > 0$ and down for $y < 0$. We further assume that

$$\mathcal{C} = \{(x, y, z) \in \mathbb{R}^3 \mid y = 0\}. \tag{5.8}$$

To specify the flow further we consider a helix Γ of radius 1 in $\mathbb{R}^3$ given by

$$\Gamma = \Gamma(\theta) = \{(x, y, z) \in \mathbb{R}^3 \mid x = \theta, y = \cos\theta,\ z = \sin\theta\} \tag{5.9}$$

with period 2π as parametrized by $\theta \in \mathbb{R}$. We assume that the flow leaves Γ invariant. Notice that Γ spirals around C and intersects Σ in infinitely many points for $|s| < 1$.

The next step of the construction is to consider a one-parameter family of invariant tubes around Γ. To obtain a generic situation, the radius (around the respective points of Γ) of the tube must vary with the angular parameter θ. We consider here a standard tube that consists of circles of radius $k\,r(\theta)$ that lie in the plane spanned by the normal $N(\theta)$ and the binormal $B(\theta)$ of Γ at $x = \theta$. The parameter k is the 'gross radius' in the sense that changing k changes the size of the tube but not its shape, which is given by $r(\theta)$; note that k plays the same role geometrically as the injection strength K in the laser system (4.5). We assume that $r(\theta)$ is generic, that is, there are no extra periodicity or symmetries. Furthermore, $r(\theta)$ is such that there are no self-intersections and other bifurcations such as saddle transitions too near the bifurcation point. A function $r(\theta)$ that satisfies all conditions with the exact formula of $\mathbb{T}$ can be found in Appendix A.

The helix Γ and the tube $\mathbb{T}$ are shown in figure 17 for three different values of k. Also shown are the section $\Sigma = \Sigma_{-0.1804} = \{(x, y, z) \in \mathbb{R}^3 \mid z = -0.1804\}$ and the extended critical locus $\mathcal{C}$. The value $s = -0.1804$ for the height of the section Σ was determined so that there is a cubic tangency bifurcation for the fixed value $k = 0.2$; namely it occurs at $\theta = 6.94193$. The intersection curves $\mathbb{T}_\Sigma$ and $\mathbb{T}_\mathcal{C}$ in Σ and $\mathcal{C}$, respectively, are shown in figure 18. In figures 17 and 18 the rows (a)–(c) show the situation before, at and after the bifurcation. Figures 17 and 18 also show the critical locus D of $\mathcal{C}$. Since we do not specify an underlying flow, the curve D must also be constructed in a consistent way. In particular, D must go through the point of cubic tangency and be consistent with the positions of $\mathbb{T}_\mathcal{C}$. These requirements are met by D as defined in Appendix A, where the flow through $\mathcal{C}$ is in the direction of negative y above D and in the direction of positive y below D.

As can be seen from figures 17 and 18 together, the planes Σ and $\mathcal{C}$, the tangency locus D and the invariant objects Γ and $\mathbb{T}$ form a consistent geometrical model for the cubic tangency bifurcation. By consistency we mean here that the conditions we place on the unspecified flow during the geometric construction are such that they can be realized by an actual flow; compare with figure 16. As for the laser system in section 5.1, the bifurcation is unfolded by changing the gross radius of the invariant manifold $\mathbb{T}$, as specified by the parameter k in (A.1). (Note that the cubic tangency bifurcation could also be unfolded by moving the section, that is, by changing the parameter s in (5.6).) The key feature in the section Σ is the single closed component $\mathbb{T}_\Sigma$ that surrounds three points $\gamma_1, \gamma_2, \gamma_3 \in \Gamma_\Sigma$; see figure 18 (left column). Before the bifurcation the closed component of $\mathbb{T}_\Sigma$ has four intersections with C; at the cubic tangency bifurcation the two innermost of them come together to a single point; and after the bifurcation there are only two intersection points (which is the minimal number for a component of $\mathbb{T}_\Sigma$ that surrounds three points of Γ_Σ). In the plane $\mathcal{C}$ the object of interest is the single closed component $\mathbb{T}_\mathcal{C}$ that surrounds only two points $\overline{\gamma}_1, \overline{\gamma}_2 \in \Gamma_\mathcal{C}$; see figure 18 (right column). Before the bifurcation the closed component of $\mathbb{T}_\mathcal{C}$ has four intersection with $\Sigma \cap \mathcal{C}$ (note that the situation in row (a) is close to a saddle transition), at the cubic tangency bifurcation the two innermost of them come together to a single point, and after the bifurcation there are only two intersection points (which is again the minimal number for a component of $\mathbb{T}_\mathcal{C}$ that surrounds two points of $\Gamma_\mathcal{C}$).

Indeed the geometric model is as simple as possible if one considers a cubic tangency bifurcation of an invariant manifold in the form of an invariant tube. The key

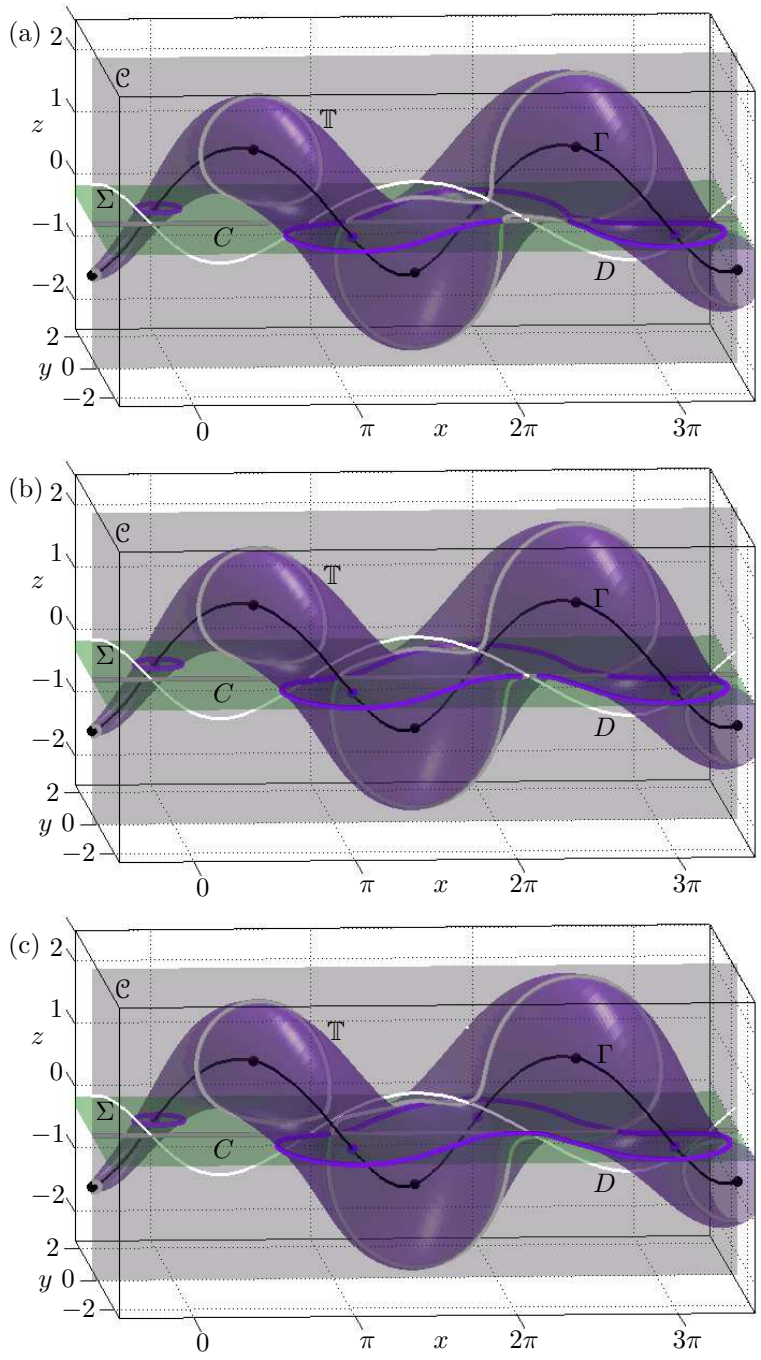

FIG. 17. *Geometrical model of a cubic tangency bifurcation, consisting of a helical orbit* Γ *surrounded by a tube* $\mathbb{T}$ *of varying radius that spiral around the tangency locus* C *of a section* Σ*; also shown is the extended critical locus* $\mathcal{C}$*. Panels (a)–(c) are before at and after the bifurcation, namely for* $k = 0.19, 0.2,$ *and* 0.21*, while the section is given by* $z = -0.1804$*; see also figure 18.*

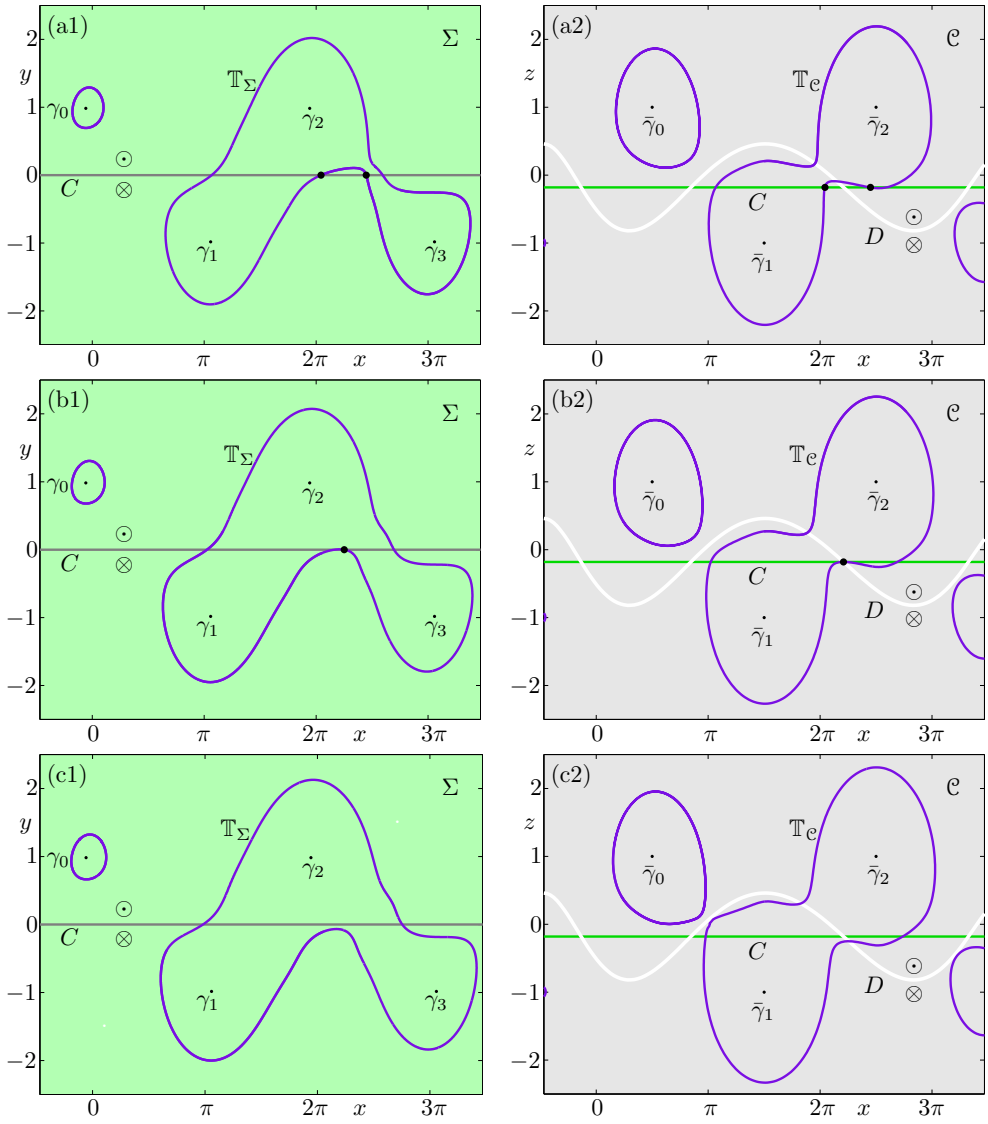

FIG. 18. *The geometrical model of a cubic tangency bifurcation shown in the section* Σ *(left column) and in the plane* $\mathcal{C}$ *(right column). Panels (a)–(c) are before at and after the bifurcation, namely for* $k = 0.19, 0.2,$ *and* 0.21*; see also figure 17.*

ingredient for this bifurcation is that the flow makes one full rotation around C, as is expressed by three intersections of the helix (periodic orbit) Γ with the section Σ. At the same time, the flow makes only half a rotation with respect to the extended critical locus $\mathcal{C}$.

5.3. Normal form of the cubic tangency bifurcation. To obtain the normal form of the cubic tangency bifurcation in a three-dimensional flowbox we consider a small neighborhood of the bifurcation in phase space. The idea is then to 'untwist' the helical structure of the flow that was identified as crucial in the geometric model in section 5.2. In other words, the flow becomes parallel and the section Σ and the

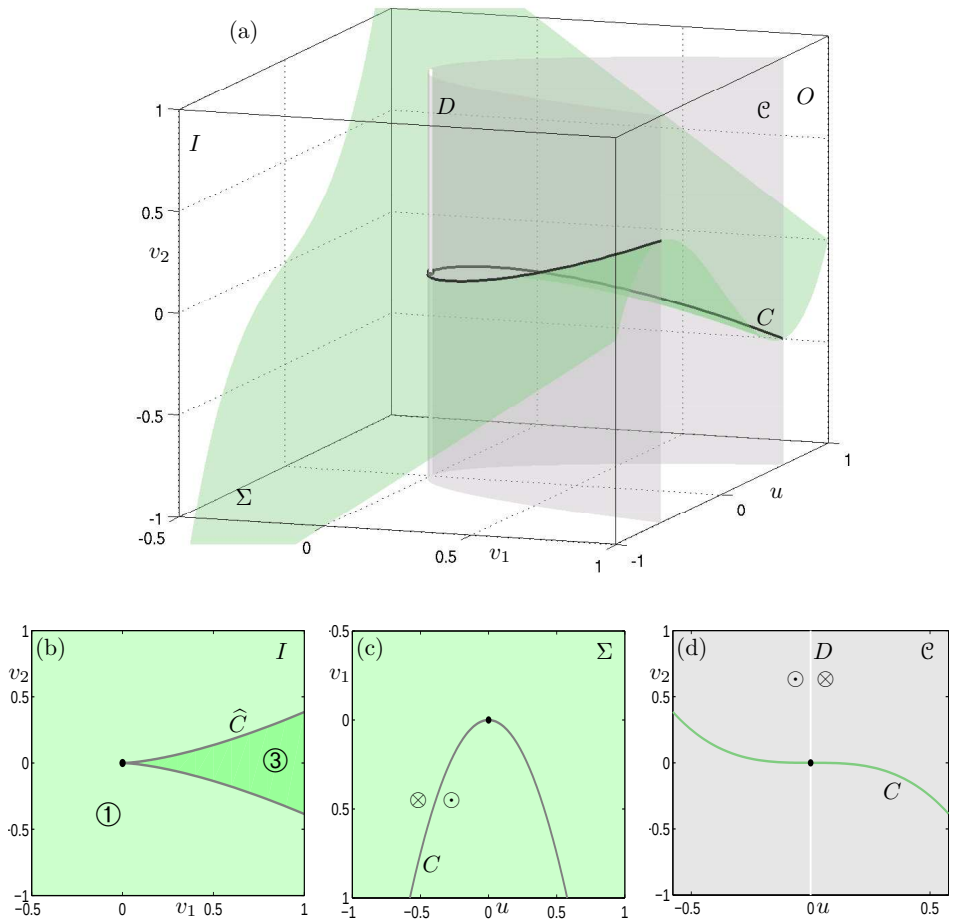

FIG. 19. *Panel (a) depicts the cuspidal section $\Sigma = \Sigma_0$ (green) of (5.11) and the extended critical locus $\mathcal{C}$ inside the standard flowbox. Panel (b) shows the projection of C and Σ onto the in-set I; the symbols ① and ③ indicate the regions with one and three intersections with Σ, respectively. Panel (c) shows the curve C in Σ, and panel (d) the the curves C and D. The direction of the flow is indicated by the symbols $\odot$ and $\otimes$.*

extended critical locus $\mathcal{C}$ deform to smooth surfaces, rather than planes.

The key realization is that, owing to the cubic tangency of the orbit involved, in the normal form one needs to consider a section Σ that has a cusp singularity with respect to the in-set I (or the out-set O). The result in the absence of an invariant manifold was proved by Sotomayor and Teixeira [32, figure 5.2] in the context of vector fields on a three-dimensional manifold with a codimension-one boundary. It can be phrased as follows in the present context.

PROPOSITION 5.1. *In any sufficiently small flowbox the phase portrait near a cubic tangency of an orbit of a flow in $\mathbb{R}^3$ with a Poincaré section is topologically equivalent to the phase portrait in the standard flowbox (2.7) for $n = 3$ given by the section*

$$\Sigma = \{(u, v_1, v_2) \in \mathbb{R}^3 \mid v_1\, u - u^3 + v_2 = 0\}. \tag{5.10}$$

In order to understand the geometry of the flow in the standard flowbox and to help make the link with the previous sections, we now construct the extended tangency locus $\mathcal{C}$. Since $\vec{n}_\Sigma((0,0,0)) = (0,0,1)$, we embed the section Σ of (5.10) into the one-parameter family of sections

$$\Sigma_s = \{(u, v_1, v_2 + s) \in \mathbb{R}^3 \mid v_1\, u - u^3 + v_2 = 0\}, \tag{5.11}$$

so that $\Sigma = \Sigma_0$. One readily finds that the tangency locus of Σ_s is

$$C = C(s) = \{(u, v_1, v_2 + s) \in \Sigma_s \mid v_1 = 3u^2,\, v_2 = -2u^3\}. \tag{5.12}$$

The projection $\widehat{C}$ of C onto the in-set I along the u-direction (the direction of the flow) has two branches that meet at a cusp point at $(v_1, v_2) = (0, s) \in I$. It follows that the extended critical locus $\mathcal{C}$ of the family Σ_s is the parabolic surface

$$\mathcal{C} = \{(u, v_1, v_2) \in \mathbb{R}^3 \mid v_1 = 3u^2\}. \tag{5.13}$$

Furthermore, the flow is tangent to $\mathcal{C}$ along the tangency locus

$$D = \{(u, v_1, v_2) \in \mathcal{C} \mid u = 0,\, v_1 = 0\},$$

where the flow is directed into the parabolic cylinder bounded by $\mathcal{C}$ for $u < 0$ and out of the parabolic cylinder for $u > 0$.

Figure 19(a) shows the section $\Sigma = \Sigma_0$ and the extended critical locus $\mathcal{C}$ inside the standard flowbox. Figure 19(b)–(d) show respective images on I, Σ and $\mathcal{C}$. The projection curve $\widehat{C}$ divides the in-set I into two regions, labeled ① and ③ in figure 19(b). Any orbit starting inside region ③ of I has three intersections with Σ while it 'winds around' the curve C in (u, v_1, v_2)-space. (Rather, in the flowbox C winds around the straight orbit segment.) Similarly, any orbit with $v_1 > 0$ intersects the parabolic surface $\mathcal{C}$ twice; compare with figure 19(d). In other words, the geometry shown in figure 19 is indeed locally diffeomorphic to that near a cubic tangency as discussed in sections 5.1 and 5.2.

PROPOSITION 5.2. *In any sufficiently small flowbox, the unfolding of a cubic tangency of a two-dimensional invariant manifold of a flow in $\mathbb{R}^3$ with a Poincaré section is topologically equivalent to the unfolding in the standard flowbox (2.7) for $n = 3$ given by the one-parameter family of sections defined in (5.11), where the invariant manifold is the plane*

$$M = \{(u, v_1, v_2) \mid v_1 = -v_2\}. \tag{5.14}$$

Proof. Suppose that the unfolding parameter of the quadratic tangency is η and the bifurcation takes place for $\eta = 0$. According to Proposition 5.1, any phase portrait of the unfolding in a flowbox near the cubic tangency point is topologically equivalent to that given by $\Sigma = \Sigma_0$ in the standard flowbox (2.7) for $n = 3$. Therefore, the invariant manifold is mapped to a surface $\widetilde{M}(\eta)$. By genericity the manifold $\widetilde{M}(0)$ is in general position, meaning that the tangent vector to $\widetilde{M}(0) \cap I$ at the origin $(v_1, v_2) = (0, 0) \in I$ has both a v_1- and a v_2-component. Due to genericity of the dependence on η the same is true for $\widetilde{M}(\eta) \cap I$ for sufficiently small η. Hence, for sufficiently small η the curve $\widetilde{M}(\eta) \cap I$ intersects the v_2-axis of I at a well-defined height $s(\eta)$, where

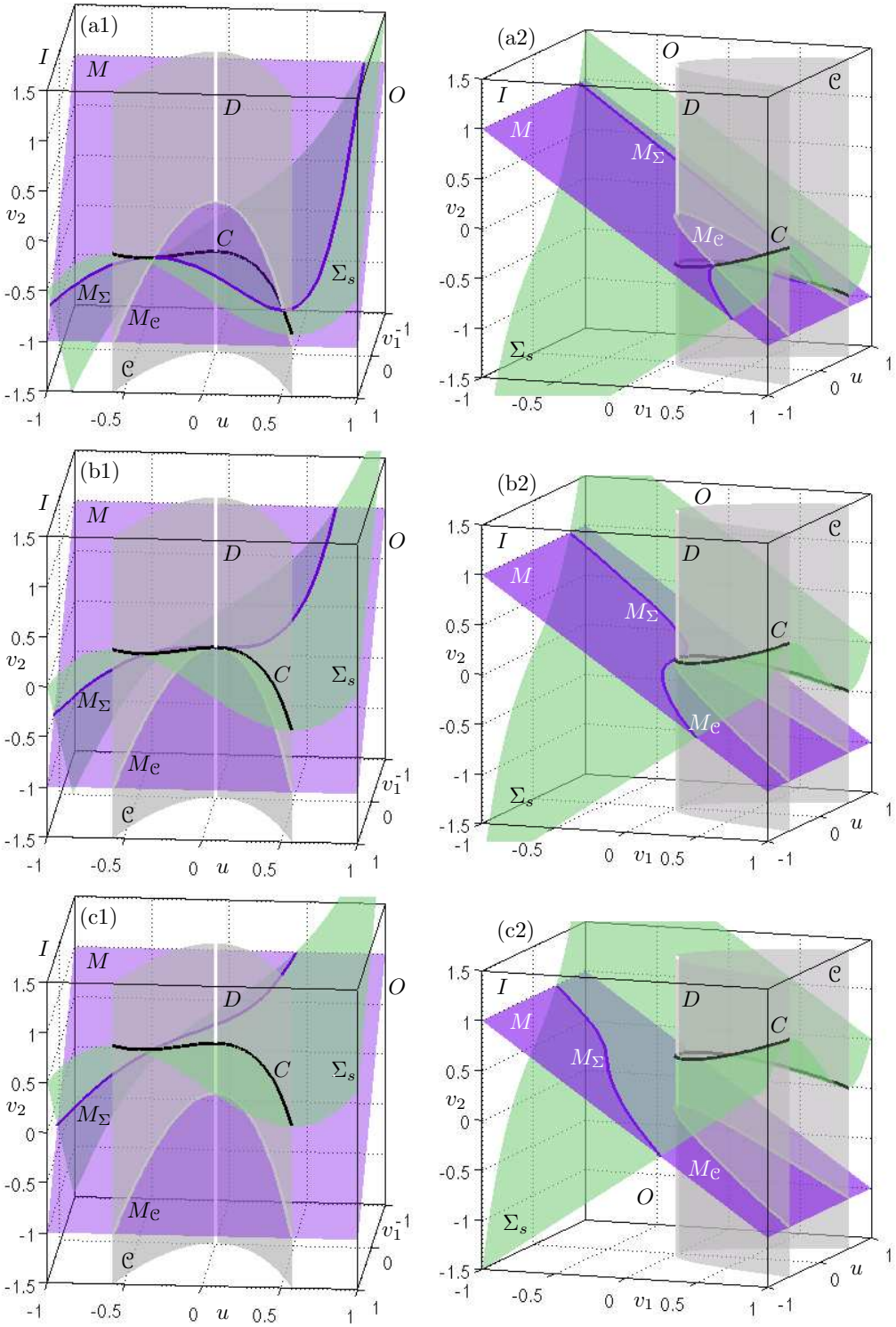

FIG. 20. *Unfolding of the cubic tangency bifurcation in normal form in the standard flowbox, presented from two different view points. Rows (a)–(c) show the invariant manifold M (purple), the section Σ_s (green) and the extended critical locus $\mathcal{C}$ (gray) before, at and after the bifurcation. Also shown are the tangency loci C and D. From (a)–(c) $s = -0.5$, $s = 0$, and $s = 0.5$; see also figure 21 and animation jcko_a3.gif.*

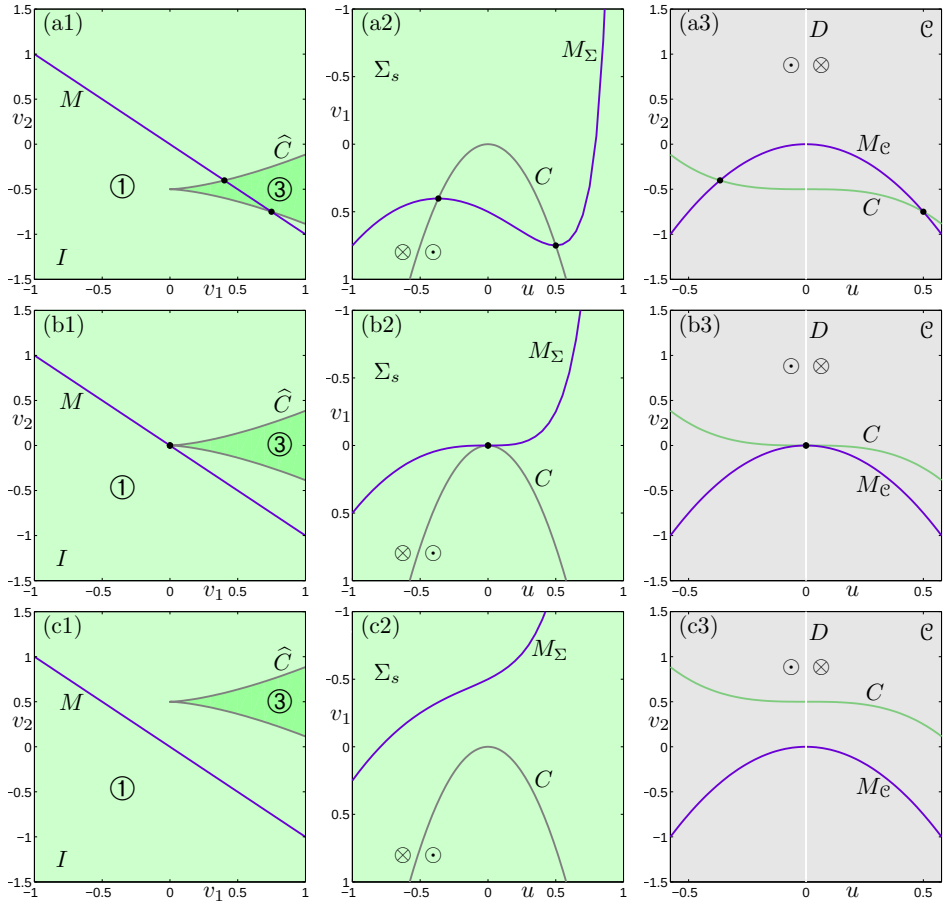

FIG. 21. *Unfolding of the cubic tangency bifurcation presented on the in-set I (left column), on the section Σ_s (middle column), and on extended critical locus $\mathcal{C}$ (right column); compare with figure 19. From (a)–(c) $s = -0.5$, $s = 0$, and $s = 0.5$; see also figure 20 and animation jcko_a3.gif.*

$s(0) = 0$; furthermore, genericity of the dependence on η implies $\frac{ds}{d\eta}(0) \neq 0$. Therefore, assuming $\frac{d\mu}{d\eta}(0) < 0$ without loss of generality, the u-independent coordinate change

$$(v_1, v_2) \mapsto (v_1, -s(\eta) - v_1 - \mu(v_1))$$

maps $\widetilde{M}(\eta)$ to M as given by (5.14). Importantly, $\frac{d\mu}{d\eta}(0) \neq 0$ implies that the image $\widetilde{\Sigma}(\eta)$ of Σ under this coordinate change is a surface with a generic cusp at $(u, v_1, v_2) = (0, 0, -s(\eta))$. As in the proof of Proposition 4.2, the surface $\widetilde{\Sigma}(\eta)$ can be brought to the required form (5.11) by a u-independent coordinate change that leaves M invariant. The overall η-family of coordinate changes is continuous by the genericity assumption on η. □

The important realization is that the manifold M of the normal form in the standard flowbox needs to be in general position relative to the cusp surface, which means that it must have non-negative components in both the v_1- and the v_2-directions. This is ensured by the choice of the 'diagonal' manifold M defined in (5.14). Note that a horizontal manifold (given by $v_2 = 0$) would always intersect the curve C in exactly

one point, while a vertical manifold (given by $v_1 = 0$) would always intersect C at the cusp point. Both situations are not generic. Furthermore, for generic M as given in the normal form by (5.14), the cubic tangency bifurcation can alternatively be unfolded by moving the manifold M up and down. This is exactly the mechanism leading to a cubic tangency of an invariant torus when its gross radius changes as in sections 5.1 and 5.2.

In figure 20 the unfolding given by Proposition 5.2 is presented in (u, v_1, v_2)-space, and in figure 21 on the in-set I, the section Σ_s and the extended critical locus $\mathcal{C}$; see also the accompanying animation jcko_a3.gif. Before the cubic tangency bifurcation the invariant manifold M_Σ in Σ_s has two intersections with the curve C. Similarly, the intersection curve $M_\mathcal{C}$ in $\mathcal{C}$ intersects C twice. At the moment of bifurcation both M_Σ and $M_\mathcal{C}$ have quadratic tangencies with C in Σ_s and $\mathcal{C}$, respectively. Notice that these tangencies indeed occur at the point $C \cap D$ as noted previously. After the bifurcation neither M_Σ nor $M_\mathcal{C}$ intersect C.

Figure 20 illustrates how this unfolding comes about by the intersection of the two-dimensional manifold M with the family of cusp surfaces Σ_s in the standard flowbox. These three-dimensional renderings indeed correspond to the respective panels in figure 21. The comparison of figure 21 with the corresponding figure 16 of a cubic tangency bifurcation in the semiconductor laser system (4.5) demonstrates how the unfolding manifests itself in a concrete example. Indeed, the unfoldings agree when one restricts attention to a sufficiently small neighborhood of the bifurcation point. While it is harder to see, this is of course also the case for the organization of the two-dimensional manifolds; compare figures 15, 17 and 20.

6. Tangency bifurcations in higher dimension and of higher codimension. The unfoldings in the previous sections of the codimension-one tangency bifurcations of a manifold M with a Poincaré section Σ of flows in $\mathbb{R}^2$ and $\mathbb{R}^3$ only give a hint of the many possibilities for tangency bifurcations of a fixed codimension in $\mathbb{R}^n$ for any n. The key realization is that there are two 'sources' of codimension: the order of contact with Σ of the orbit $\mathcal{O}(\mathbf{x}^*)$ of the tangency point $\mathbf{x}^*$, and possible codimension associated with tangencies of M and Σ at $\mathbf{x}^*$ in other directions. The first example of a tangency bifurcation with both types of tangencies is the codimension-one quadratic tangency in $\mathbb{R}^3$ in section 4.

Classifying and unfolding tangency bifurcations of higher codimension and for $n > 3$ is beyond the scope of this paper. However, we now give a general framework for this task, which is based on a more detailed consideration of the intersection of the tangent spaces $T_M(\mathbf{x}^*)$ and $T_\Sigma(\mathbf{x}^*)$.

DEFINITION 6.1. *Let M be an invariant manifold of dimension ℓ of a vector field f on $\mathbb{R}^n$ with a given planar $(n-1)$-dimensional global Poincaré section Σ. Suppose that the following conditions are satisfied:*

- *(B1) there is a point $\mathbf{x}^* \in M \cap \Sigma$ such that the orbit $\mathcal{O}(\mathbf{x}^*)$ has a tangency of degree $d \in \mathbb{N}$ with Σ at $\mathbf{x}^*$, where we assume that the tangency is at least quadratic, that is, $d \geq 2$;*
- *(B2) The dimension of the orthogonal complement N of $f(\mathbf{x}^*)$ in $T_M(\mathbf{x}^*) \cap T_\Sigma(\mathbf{x}^*)$ is p; and*
- *(B3) The point $\mathbf{x}^*$ is a critical point of codimension q of the map from N to M.*

Then we say that M and Σ have a d-tangency with singularity dimension p and singularity codimension q *at $\mathbf{x}^*$ (or d-p-q-tangency or short).*

The singularity codimension q is only defined for $p > 0$, meaning that $p = 0$ iff $q = 0$. Furthermore, by construction of N there must be a tangency (quadratic or

of higher degree) along each of the base vectors of N, so that $q \geq p$. From the data specified in Definition 6.1 one can determine the overall codimension.

PROPOSITION 6.2. *The codimension c of a d-p-q-tangency of an ℓ-dimensional invariant manifold $M \subset \mathbb{R}^n$ with a global Poincaré section is $c = d + q - \ell$, where $p < \ell < n$.*

Proof. Generically, $\dim(\Sigma \cap M) = \ell - 1$, independently of n. Furthermore, by (B1) and (B3) the point $\mathbf{x}^*$ is a critical point of codimension $(d-1)+q$ of the map from $T_M(\mathbf{x}^*) \cap T_\Sigma(\mathbf{x}^*)$ to M. Therefore, the codimension of the bifurcation is $c = (d-1) + q - (l-1)$. □

Proposition 6.2 has some interesting immediate consequences. First of all, it shows that we indeed presented all codimension-one d-p-q-tangency bifurcations for $n \leq 3$, namely:

1. the 2-0-0-tangency for $\ell = 1$ is the quadratic tangency of a one-dimensional manifold in $\mathbb{R}^2$ and in $\mathbb{R}^3$ of Proposition 3.2 and Corollary 4.1, respectively;
2. the 2-1-1-tangency for $\ell = 2$ is the quadratic tangency of a two-dimensional manifold in $\mathbb{R}^3$ of Proposition 4.2; and
3. the 3-0-0-tangency for $n = 3$ and $\ell = 2$ is the cubic tangency of a two-dimensional manifold in $\mathbb{R}^3$ of Proposition 5.2.

Similarly, one can easily list all codimension-two tangency bifurcations for $n \leq 3$, which are:

1. the 3-0-0-tangency for $\ell = 1$ is the cubic tangency of a one-dimensional manifold in $\mathbb{R}^2$ and in $\mathbb{R}^3$;
2. the 2-1-2-tangency for $\ell = 2$ is the quadratic tangency of a two-dimensional manifold with a cubic tangency in the one-dimensional N-direction;
3. the 3-1-1-tangency for $\ell = 2$ is the cubic tangency of a two-dimensional manifold with a quadratic tangency in the one-dimensional N-direction.
4. the 4-0-0-tangency for $\ell = 2$ is the quartic tangency of a two-dimensional manifold.

An important new element of codimension-two tangency bifurcations is that they cannot be unfolded solely by moving the section Σ (because Σ is of codimension one in $\mathbb{R}^n$). Of the cases above, only the unfolding for $\ell = 1$, that is, the codimension-two cubic 3-0-0-tangency, is straightforward.

PROPOSITION 6.3. *In any sufficiently small flowbox, the unfolding of a cubic tangency of a one-dimensional invariant manifold of a flow in $\mathbb{R}^3$ with a global Poincaré section is topologically equivalent to the unfolding in the standard flowbox (2.7) for $n = 3$ given by the one-parameter family of sections (5.11) that interacts with the one-parameter family of manifolds*

$$M = \{(u, v_1, v_2) \mid v_1 = \lambda \text{ and } v_2 = 0\}.$$

This result follows from Proposition 5.1 in the same way as Proposition 3.2 follows from Proposition 3.1, namely by the construction of a parameter-dependent coordinate change. Proposition 6.3 says that the unfolding of the codimension-two cubic tangency of a one-dimensional manifold in $\mathbb{R}^3$ (and, therefore, in all dimensions $n \geq 2$ and including $n = 2$) is given by the standard unfolding of a cusp bifurcation. Namely, the phase portrait is determined by the relative position of the point $M_I = (0, \lambda)$ in the in-set I relative to projection $\widehat{C}(s)$ of the fold curve; see figure 19. Crossing one of the two branches of $\widehat{C}(s)$ corresponds to a codimension-one quadratic tangency that

unfolds as given by Corollary 4.1. At the central codimension-two point the manifold passes exactly through the cusp point in I.

Suppose now that M is actually a segment of a periodic orbit Γ, meaning that there is a global return R from the out-set O back to the in-set I that leaves M invariant. Then the number of intersections of Γ with Σ changes by two when Γ crosses C, even if this happens at the cusp point.

7. Conclusions and discussion. We considered the class of tangency bifurcations, which are bifurcations that one finds generically in global Poincaré maps but that are not due to bifurcations of the underlying vector field. Tangency bifurcations involve the interaction of an invariant manifold with the tangency locus of the section, which is non-empty unless the system is effectively periodically forced. Specifically, we presented a complete treatment of codimension-one tangency bifurcations of flows in $\mathbb{R}^2$ and $\mathbb{R}^3$, that is, for one-dimensional and two-dimensional Poincaré sections. We constructed their normal forms in the standard flowbox by specifying suitable families of curved smooth sections that interact with straight invariant manifolds of appropriate dimension. Our approach is similar in spirit to that taken by Sotomayor and Teixera, who considered flows on manifolds with one and two-dimensional boundaries. However, depending on the dimensions involved, further coordinate transformations are required to 'straighten out' the invariant manifold.

With the examples of the two-dimensional unforced Van der Pol oscillator and a three-dimensional model of a semiconductor laser with optical injection we demonstrated how the codimension-one tangency bifurcations manifest themselves in a specific vector field. Namely, we studied the interactions of periodic orbits and invariant tori with the tangency locus of a given planar section. As is the case generically, the respective bifurcations of the Poincaré map can be brought about by either changing some system parameter of by moving the section. The quadratic tangencies of one- or two-dimensional invariant manifolds with a planar section could be associated with the respective normal forms in the flowbox in a relatively straightforward manner. In the case of a cubic tangency, on the other hand, the operation of 'straightening out' the flow to obtain the normal form in the flowbox is quite complicated. Therefore, a simplified geometric model at an intermediate step was constructed to help understand the normal form transformation geometrically.

The unfoldings presented here were shown to fit naturally into a general framework for the classification of tangency bifurcations of arbitrary codimension. The general idea is that a tangency of degree $d \geq 2$ of an orbit on the manifold is accompanied by other possible tangencies of the manifold in the directions normal to this orbit. This point of view provides a clear direction for the future study of tangency bifurcations in higher-dimensional spaces and of higher codimension. We already listed the codimension-two tangency bifurcations of a two-dimensional manifold in $\mathbb{R}^3$, and the construction of their unfoldings is an interesting challenge. Another important next step and the subject of our ongoing research is the study of tangency bifurcations in $\mathbb{R}^4$. This study naturally starts with the tangency bifurcations of codimension one, as they are encountered naturally when a single parameter of the vector field is changed, or the section is moved. The normal forms that need to be developed involve intersections of hypersurfaces in $\mathbb{R}^4$, which is very hard to imagine and visualize. This difficulty can be overcome by considering the corresponding surfaces in the three-dimensional in-set of the flow box. Note that it will be a real challenge to identify and visualize tangency bifurcations in three-dimensional Poincaré sections in concrete vector fields arising from applications.

Another topic of ongoing research is the classification of different mechanisms in which points or regions are created in the Poincaré section for which the flow never returns back to the section. In other words, the issue is to find bifurcations that create new sets of the section where the Poincaré map is not defined. As we already demonstrated in section 3.3, such bifurcations may be due to interactions between the Poincaré section and stable and unstable manifolds of equilibria and other invariant sets that do not lie in the section. Already for the case of three-dimensional flows, the study of these bifurcations in applications requires the use of numerical techniques for the computation of two-dimensional global invariant manifolds, such as those in [11, 21, 22].

Finally, we mention a related subject: the study of bifurcations of a Poincaré map that are due to the passage of an equilibrium of the flow through the section. As for tangency bifurcations, this does not correspond to a bifurcation of the underlying vector field. The added difficulty is that is not possible in this situation to consider a normal form in a flowbox (which cannot contain equilibria). A natural starting point for ongoing research are the codimension-one bifurcations of a Poincaré map where a hyperbolic equilibrium passes through the section; the type of bifurcation and its unfolding obviously depend on the topological type of the equilibrium.

REFERENCES

[1] H. Abarbanel, L. Korzinov, A. Mees, and N. Rulkov, *Small force control of nonlinear systems to given orbits*, IEEE Transactions on Circuits and Systems I: Fundamental Theory and Applications, 44 (1997), pp. 1018–1023.

[2] V. I. Arnol′d, *Catastrophe Theory*, Springer-Verlag, 3rd ed., 1992.

[3] G. D. Birkhoff, *Dynamical systems with two degrees of freedom*, Trans. Am. Math. Soc., 18 (1917), pp. 199–300.

[4] A. Bolsinov, H. R. Dullin, and A. Wittek, *Topology of energy surfaces and existence of transversal Poincaré sections*, J. Phys. A: Math. Gen., 29 (1996), pp. 4977–4985.

[5] H. Broer, I. Hoveijn, M. van Noort, C. Simó, and G. Vegter, *The parametrically forced pendulum: A case study in 1 1/2 degree of freedom*, J. Dyn. Diff. Equ., 16 (2004), pp. 897–947.

[6] W.-C. Chan, *A note on diffeomorphism and periodic differential equations*, Mathematical and Computer Modelling, 36 (2002), pp. 1387–1392.

[7] D. Chillingworth, *Discontinuity geometry for an impact oscillator*, Dynamical Systems, 17 (2002), pp. 389–420.

[8] P. Collins and B. Krauskopf, *Entropy and bifurcations in a chaotic laser*, Phys. Rev. E, 66 (2002), p. 056201.

[9] H. R. Dullin and A. Wittek, *Complete Poincaré sections and tangent sets*, J. Phys. A: Math. Gen., 28 (1995), pp. 7157–7180.

[10] J. P. England, B. Krauskopf, and H. M. Osinga, *Bifurcations of stable sets in noninvertible planar maps*, Int. J. Bifurcation and Chaos, 15 (2005), pp. 891–904.

[11] ———, *Computing one-dimensional global manifolds of Poincaré maps by continuation*, SIAM J. App. Dyn. Sys., 4 (2005), pp. 1008–1041.

[12] G. O. Fountain, D. V. Khakhar, and J. M. Ottino, *Visualization of three-dimensional chaos*, Science, 281 (1998), pp. 683–686.

[13] M. Golubitsky and D. G. Schaeffer, *Singularities and Groups in Bifurcation Theory*, vol. 1, Springer-Verlag, 1985.

[14] K. Green and B. Krauskopf, *Global bifurcations and bistability at the locking boundaries of a semiconductor laser with phase-conjugate feedback*, Phys. Rev. E, 66 (2002), p. 016220.

[15] J. Guckenheimer and P. Holmes, *Nonlinear Oscillations, Dynamical Systems, and Bifurcations of Vector Fields*, Springer-Verlag, 1983.

[16] I. Gumowski and C. Mira, *Recurrences and Discrete Dynamic Systems*, Springer-Verlag, 1980.

[17] J. Hale and H. Koçak, *Dynamics and Bifurcations*, Springer-Verlag, 1991.

[18] M. Hirsch and S. Smale, *Differential Equations, Dynamical Systems, and Linear Algebra*, Academic Press, 1974.

[19] C. Jung, T. H. Seligman, and J. M. Torres, *Canonically transformed detectors applied to the classical inverse scattering problem*, J. Nonlin. Math. Phys., 12 (2005), p. 404.
[20] W. Just and H. Kantz, *Some considerations on Poincaré maps for chaotic flows*, J. Phys. A: Math. Gen., 33 (2000), pp. 163–170.
[21] B. Krauskopf and H. M. Osinga, *Computing geodesic level sets on global (un)stable manifolds of vector fields*, SIAM J. App. Dyn. Sys., 2 (2003), pp. 546–569.
[22] B. Krauskopf, H. M. Osinga, E. Doedel, M. Henderson, J. Guckenheimer, A. Vladimirsky, M. Dellnitz, and O. Junge, *A survey of methods for computing (un)stable manifolds of vector fields*, Int. J. Bifurcation and Chaos, 15 (2005), pp. 763–791.
[23] B. Krauskopf, H. M. Osinga, and B. B. Peckham, *Unfolding the cusp-cusp bifurcation of planar endomorphisms*, SIAM J. App. Dyn. Sys., 6 (2007), pp. 403–440.
[24] Y. A. Kuznetsov, *Elements of Applied Bifurcation Theory*, Springer-Verlag, 2004.
[25] E. H. Lockwood, *A Book on Curves*, Cambridge University Press, 1961.
[26] Z. Nitecki, *Differentiable Dynamics*, MIT Press, 1971.
[27] J. Palis and W. de Melo, *Geometric Theory of Dynamical Systems*, Springer-Verlag, 1982.
[28] R. Peikert and F. Sadlo, *Eurographics/IEEE-VGTC Symposium on Visualization*, The Eurographics Association, 2007, ch. Visualization methods for vortex rigs and vortex breakdoen bubbles.
[29] ———, *Topology-based Methods in Visualization*, Springer-Verlag, 2007, ch. Flow topology beyond skeletons: visualization of features in recirculating flow.
[30] H. Poincaré, *Les Méthodes Nouvelles de la Mécanique Céleste*, Paris: Gauthier-Villars, 1892-1899. Translated: *New Methods of Celestial Mechanics* 1993.
[31] M. G. Rosenblum, A. S. Pikovsky, and J. Kurths, *Phase synchronization of chaotic oscillators*, Phys. Rev. Lett., 76 (1996), p. 1804.
[32] J. Sotomayor and M. A. Teixeira, *Dynamical Systems Valparaiso 1986*, vol. 1331 of Lecture Notes in Mathematics, Springer–Verlag, 1988, ch. Vector fields near the boundary of a 3–manifold, pp. 169–195.
[33] S. H. Strogatz, *Nonlinear Dynamics and Chaos: With applications to Physics, Biology, Chemistry, and Engineering*, Addison-Wesley, 1994.
[34] M. A. Teixeira, *Generic bifurcation in manifolds with boundary*, J. Diff. Equ., 25 (1977), pp. 65–89.
[35] E. W. Weisstein, *CRC Concise Encyclopedia of Mathematics*, Chapman & Hall, 2002.
[36] S. Wieczorek, B. Krauskopf, T. B. Simpson, and D. Lenstra, *The dynamical complexity of optically injected semiconductor lasers*, Physics Reports, 416 (2005), pp. 1–128.
[37] X.-S. Yang, *A remark on global Poincaré section and suspension manifold*, Chaos, Solitons and Fractals, 11 (2000), pp. 2157–2159.
[38] E. C. Zeeman, *Catastrophe Theory*, Selected papers 1972–1977, Addison-Wesley, 1977.

Appendix A. Details of the helical tube construction.

A standard tube of radius $k\,r(\theta)$ around the helix (5.9) is given by

$$\mathbb{T} = \{\Gamma(\theta) + k\,r(\theta)\,(N(\theta)\cos\phi + B(\theta)\sin\phi) \text{ for } \theta \in \mathbb{R},\ 0 \le \phi < 2\pi\}\,, \tag{A.1}$$

where $N(\theta)$ is the normal and $B(\theta)$ the binormal at $x = \theta$. From (5.9) it follows that the tangent, normal and binormal are

$$T = \left(\frac{1}{\sqrt{2}}, -\frac{\sin\theta}{\sqrt{2}}, \frac{\cos\theta}{\sqrt{2}}\right),\ N = (0, \cos\theta, \sin\theta)\,, B = \left(\frac{1}{\sqrt{2}}, \frac{\sin\theta}{\sqrt{2}}, -\frac{\cos\theta}{\sqrt{2}}\right).$$

Therefore, the helical tube (A.1) takes the form

$$\mathbb{T} = \left\{ (x,y,z) \in \mathbb{R}^3 \mid x = \theta + k\,r(\theta)\frac{\sin\phi}{\sqrt{2}}, y = \cos\theta + k\,r(\theta)\left(\cos\theta\cos\phi + \frac{\sin\theta\sin\phi}{\sqrt{2}}\right),\right.$$
$$\left. z = \sin\theta + k\,r(\theta)\left(\sin\theta\cos\phi - \frac{\cos\theta\sin\phi}{\sqrt{2}}\right),\ \text{for } \theta \in \mathbb{R},\ 0 \le \phi < 2\pi \right\}.$$

A function $r(\theta)$ that satisfies the requirements mentioned in section 5.2 is

$$r\,(\theta) = \left(\sin^2\theta - \left(\frac{2\theta - 3\pi}{2\pi}\right)^2 - \frac{1}{2}\left(\frac{4\theta - 14\pi}{7\pi}\right)^2 + \frac{4}{5}\exp\left(\frac{11\pi}{4} - \theta\right) + 6\right).$$

For $K = 0.2$ we find a cubic tangency bifurcation with the plane $\Sigma = \Sigma_{-0.1804}$ at $\mathbf{x}^* \approx (6.94193, 0, -0.1804) \in C \subset \Sigma$. The curve $D \subset \mathcal{C}$ can now be constructed by observing the condition that it goes through $\mathbf{x}^*$ and is in general position with respect to the components of $\mathbb{T}_{\mathcal{C}}$. The definition

$$D = D(\theta) = \left\{ (\theta, 0, z) \in \mathcal{C} \mid z = -0.64 \sin\left(\frac{16\theta\pi^2 - 111.0709\pi^2}{-0.34\,(2\theta - 3\pi)^2 + 22.4\pi^2} \right) + 0.1804 \right\}$$

meets these requirement, as can be seen from figure 18. Note that the choice of $r(\theta)$ and D are by no means unique. The formulae presented here are indeed quite involved, but they allow one to compute all objects of interest while being consistent with the existence of an underlying flow.